Krittika Summer Projects 2024

Eclipsing Binaries

with `PHOEBE`

Adhya, Sumit Kumar, B T, Karan, Garg Navya, Giri,
Devesh, Kotecha Dhairya, Nandi Mainak, Rajpoot,
Bhavesh, and Sahoo, Soumik

KRITTIKA SUMMER PROJECTS 2024

Eclipsing Binaries

with `PHOEBE`

Adhya, Sumit Kumar[1], B T, Karan[2], Garg Navya[1], Giri, Devesh[3], Kotecha Dhairya[4], Nandi Mainak[1], Rajpoot, Bhavesh[5], and Sahoo, Soumik[1]

[1]Indian Institute of Technology, Bombay, 400076, India

[2]National Institute of Technology Karnataka, Mangalore, 575025, India

[3]Indian Institute of Science Education and Research, Pune, 411008, India

[4]Indian Institute of Technology, Roorkee, 247667,India

[5]University of Heidelberg, 69117 Heidelberg, Germany

Copyright © 2024 Krittika IITB
PUBLISHED BY KRITTIKA: THE ASTRONOMY CLUB OF IIT BOMBAY
GITHUB.COM/KRITTIKAIITB
Sample Repository: Type project name
First Release, August 2024

Abstract (Sample abstract)

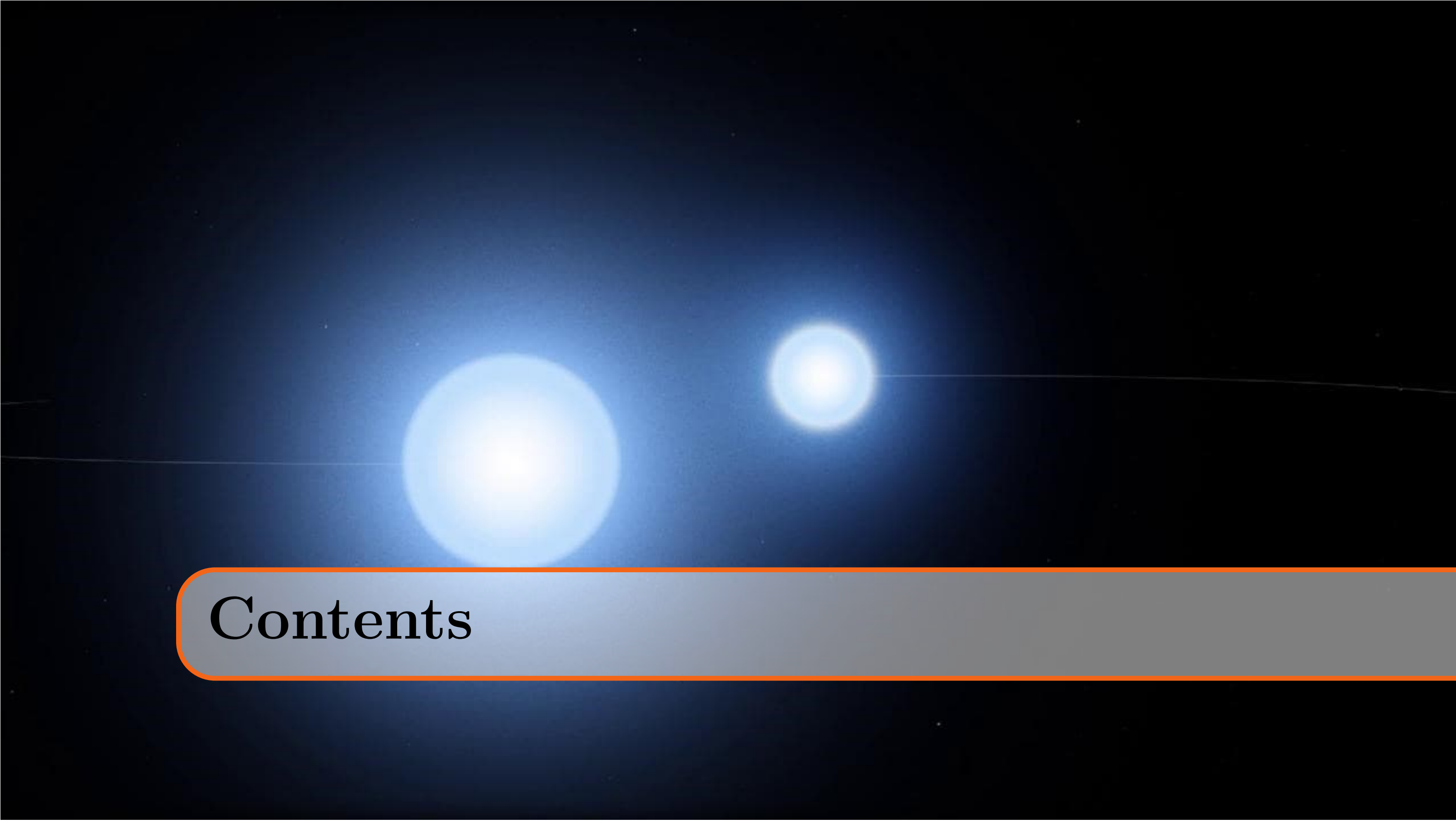

Contents

I Part One

1 Binary Star Systems 9

1.1 Historical Significance 9

1.2 Classifications 10

1.3 Importance in Astrophysics 11

1.4 Origins and Fate 12

2 Preliminaries 15

2.1 Celestial Co-ordinates, Celestial Sphere and Epochs 15

2.1.1 Celestial Co-ordinate 15

2.1.2 Epochs 16

2.1.3 Celestial Sphere 16

2.2 Fluxes, Magnitudes, and luminosity 16

2.2.1 Magnitude 16

2.2.2 Radiant flux and luminosity 16

2.2.3 Absolute magnitude 16

2.2.4 Distance modulus(μ) 17

2.3 The 2-Body Problem 17

2.3.1 Reducing the Two-Body Problem into a One-Body Problem 17

2.3.2 Determining the orbital shape, $r(\theta)$ 19

2.4 Using the 1-body analysis to solve the original 2-body problem 22

2.5 Kepler Laws and Elliptical Orbits 23

2.5.1 Kepler's Laws 23

2.5.2 Properties of elliptical orbits and orbital elements 23
2.5.3 Motion of the star system with time 26

3 **Spectroscopic Binary Stars** 29
3.1 Introduction 29
3.2 The Radial Velocity Curve 30
3.2.1 Notations and definitions 30
3.2.2 Radial velocity 31
3.3 Extracting parameters from the RV curve 32
3.3.1 Orbital and Spectroscopic parameters 32
3.4 Period 35
3.5 Refining the orbital elements 35
3.6 Summary 36
3.7 Further comments 36

4 **Eclipsing Binary Stars** 39
4.1 Introduction 39
4.1.1 Types of Eclipsing Binaries 40
4.1.2 Some important Space Missions About Eclipsing Binares 40
4.2 Astrophysical Significance 43
4.3 Observations 44
4.4 Estimation of parameters 45

II Part Two

5 **Introduction to `PHOEBE`** 53
5.1 Why use `PHEOBE` ? 53
5.2 Basics of Bundle 54
5.3 Constraints 54
5.4 Datasets 54
5.4.1 Light Curves (lc) 55
5.4.2 Radial Velocities (rv) 56
5.4.3 Line Profiles (lp) 56
5.4.4 Orbits (orb) 57
5.4.5 Meshes 58
5.5 Compute 58
5.5.1 Custom Compute Options 59
5.5.2 Temporarily Overriding Options 60
5.5.3 Alternate Backends 60
5.6 Times and Phases 60
5.6.1 Compute Phases 61

6 Forward Model . . . 63
6.1 What’s Forward Modeling? 63
6.2 Applications of Forward Modeling in Eclipsing Binaries 64
6.3 Key Steps for Forward Modeling with `PHOEBE` 65
6.3.1 Defining System Parameters: . . . 66
6.3.2 Adding dataset: . . . 67
6.3.3 Computing: . . . 67
6.3.4 Ploting: . . . 67
6.4 DI Herculis: Misaligned binary 69

7 Inverse problem . . . 73
7.1 Estimators 73
7.1.1 Periodograms . . . 74
7.1.2 RV Geometry . . . 74
7.1.3 LC Estimators . . . 75
7.2 Merit Function 79
7.3 Optimizers 80
7.4 Samplers 81
7.4.1 Markov Chain Monte Carlo (emcee) . . . 81
7.5 Posteriors & Uncertainties 83

Bibliography . . . 85

Index . . . 89

I

Part One

1 Binary Star Systems **9**
1.1 Historical Significance
1.2 Classifications
1.3 Importance in Astrophysics
1.4 Origins and Fate

2 Preliminaries **15**
2.1 Celestial Co-ordinates, Celestial Sphere and Epochs
2.2 Fluxes, Magnitudes, and luminosity
2.3 The 2-Body Problem
2.4 Using the 1-body analysis to solve the original 2-body problem
2.5 Kepler Laws and Elliptical Orbits

3 Spectroscopic Binary Stars **29**
3.1 Introduction
3.2 The Radial Velocity Curve
3.3 Extracting parameters from the RV curve
3.4 Period
3.5 Refining the orbital elements
3.6 Summary
3.7 Further comments

4 Eclipsing Binary Stars **39**
4.1 Introduction
4.2 Astrophysical Significance
4.3 Observations
4.4 Estimation of parameters

1. Binary Star Systems

A **binary star** or **binary star system** is a system of two stars that are gravitationally bound to each other and orbit a common centre of mass called a *barycenter*.

1.1 Historical Significance

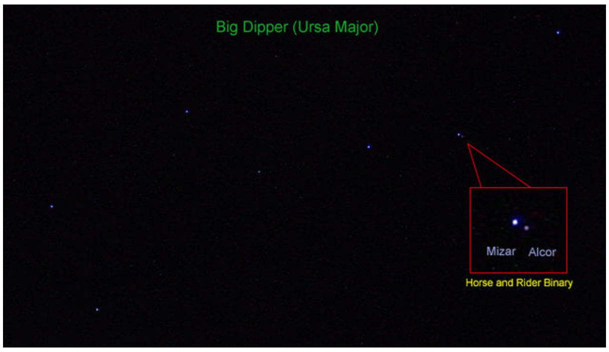

Figure 1.1: Mizar and Alcor in constellation Ursa Major

Double stars or *visual doubles*, a pair of stars that appear close to each other, have been observed since the invention of the telescope. Early examples include *Mizar* [1.1] and *Acrux* [1.2]. Evidence that stars in pairs were more than just optical alignments came in 1767 when English natural philosopher *John Michell* became the first person to apply mathematics and statistics to the study of the stars (Michell, 1767). He focused his investigation on the *Pleiades* cluster and calculated that the likelihood of finding such a close grouping of stars was about one in half a million. He concluded that the stars in these double or multiple-star systems might be drawn to one another by gravitational pull, thus providing the first evidence of binary stars and star clusters. *William Herschel* began observing double stars in 1779, and by 1803,(Herschel, 1802) he had observed changes in the relative positions of several double stars over 25 years and concluded that the

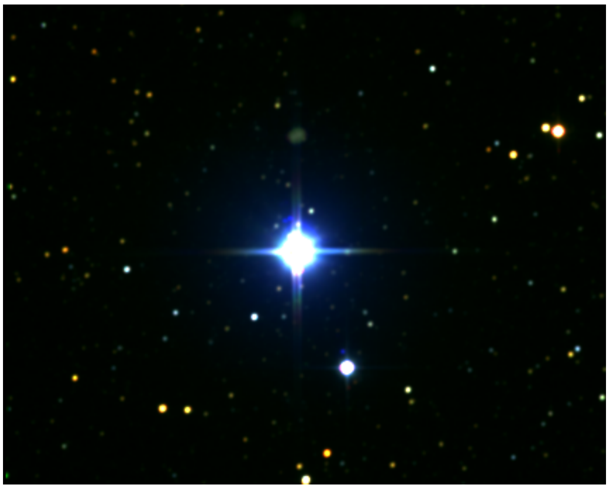

Figure 1.2: α crucis with its close companion HD 108250 (the 2nd brightest star)

stars were orbiting each other and coined the term *binary star* for stars exhibiting orbital motion towards each other. The first orbit of a binary star was computed by *Félix Savary* in 1827.

In recent years, there have been numerous double stars that have been cataloged and measured. As of June 2024, the *Washington Double Star Catalog*, a database of visual double stars compiled by the *United States Naval Observatory*, contains over 150,000 pairs of double stars, including optical doubles and binary stars. Orbits have been determined for only a few thousand of these double stars. Gaia Data Release 3 (Gaia DR3) has been released on 13 June 2022. DR3 included astrometric orbital solutions for 168,065 sources, including 134,598 with purely astrometric solutions and 33,467 joint astrometric + RV solutions, orbital solutions based purely on RVs for 181529 single-lined binaries and 5376 double-lined binaries. DR3 also included a sample of short-period binaries displaying photometric variability, including both eclipsing and ellipsoidal systems 86,918 sources have pure light curve solutions, while 155 have joint light curve + RV solutions (El-Badry, 2024). About 16,000 resolved white dwarf (WD) + main sequence (MS) binaries and 1,500 WD+WD wide binaries have been identified from Gaia data.

1.2 Classifications

Binary stars are categorized into four distinct types based on their method of observation: *visually*, through direct observation; *spectroscopically*, by detecting periodic variations in spectral lines; *photometrically*, through changes in luminosity caused by an eclipse; *astrometrically*, by measuring a deviation in star's position caused by an unseen companion. It is noteworthy that a binary star system may fall into multiple categories for instance, several spectroscopic binaries also exhibit characteristics of eclipsing binaries.

- *Visual binaries* are binary stars in the sky that are seen as a single object and often resolved using a telescope as separate stars. They are usually close to Earth and have a large orbital separation between the two components to permit them to be observed as a double star in a telescope. The double star Castor was found to be a visual binary system with a separation of 3.9" and a period of 467 years (Heintz, 1988).
- *Spectroscopic binaries* consist of a pair of stars where the spectral lines in the light

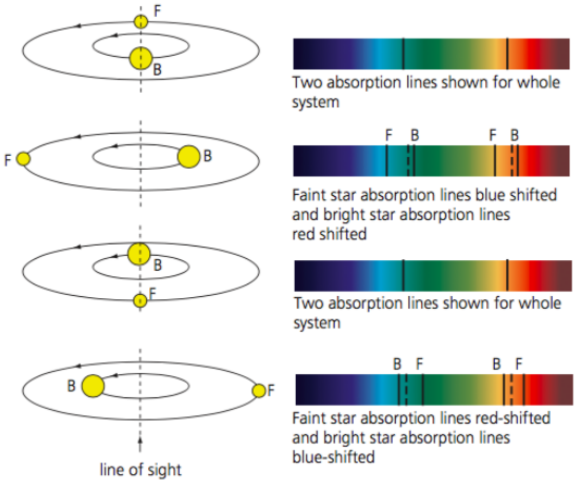
F
B
Two absorption lines shown for whole system
F
B
F B F B
Faint star absorption lines blue shifted and bright star absorption lines red shifted
B
F
Two absorption lines shown for whole system
B
F
B F B F
Faint star absorption lines red-shifted and bright star absorption lines blue-shifted
line of sight

Figure 1.3: The observed combined spectrum shows the shifting of spectral lines.

emitted from each star shift first towards the blue indicating the motion towards the observer, then away from us by shifting towards the red [1.3]. In these systems, the separation between stars is usually very small. The observed *radial velocity* of the system varies periodically due to orbital motion. Radial velocity can be measured with a spectrometer by observing the Doppler shift of the star's spectral lines. In some spectroscopic binaries, spectral lines from both stars are visible. In these cases, the lines alternate between being double and single. This type of system is known as a double-lined spectroscopic binary (SB2). In other systems, only one star's spectrum is visible, and it periodically shifts towards the blue, then towards the red, and back again. Stars in these systems are known as single-lined spectroscopic binaries (SB1).

- An *eclipsing binary* star is a binary star system in which the orbital plane of the two stars lies in the line of sight of the observer, causing the components to undergo mutual eclipses. Eclipsing binaries are variable stars not because the light of individual components varies, but because of the eclipses. The light curve of an eclipsing binary is characterized by periods of practically constant light, with periodic drops in intensity when one star passes in front of the other. These are the main focus of our study in the following sections.
- *Astrometric binaries* are stars that are relatively close and can be observed to wobble around a point in space, with no visible companion. This companion could be very faint, making it currently undetectable or obscured by the brightness of the primary star, or it could be an object that emits minimal or no electromagnetic radiation.

1.3 Importance in Astrophysics

From observations of the motion of one of the stars relative to the other, it is possible to determine several of the properties of the orbit orbital period (P) orbital eccentricity (e) the argument of periastron (ω) semi-major axis (a) (Table **??**). The semimajor axis (a) that can be found is *angular size*, not the true length. The properties such as the argument of periastron (ω), the longitude of ascending node (Ω), and orbital inclination (i) can also be measured, as these define the orientation of the orbit relative to the observer.

Hence, these are collectively known as *Orbital Parameters*.

For a "single-lined" spectroscopic binary system (SB1), we can measure the quantities $P,\ e,\ \omega,\ K_1,\ V_\gamma$ (Table **??**). From these values, we can calculate the mass function *f(M)* and a component of the semi-major axis ($a_1 sini$). For a "double-lined" spectroscopic binary system, we can obtain all the quantities for SB1 systems and, in addition, the minimum masses ($M_1 sin^3 i$ and $M_2 sin^3 i$), as well as a component of the semi-major axis ($asini$). However, without knowing the orbital inclination, the true values of these quantities are not accessible.

Eclipsing binaries are particularly valuable in the study of binary stars because they allow for the precise measurement of various physical properties. By analyzing the light curve of an eclipsing binary, we can determine its orbital period, as well as the relative sizes of the individual stars in terms of their radii. For SB2 EBs, it is possible to measure the masses, radii, and luminosities of both stars, provided they have not undergone mass transfer and evolved as single stars. This information is crucial for calibrating the theoretical stellar models.

1.4 Origins and Fate

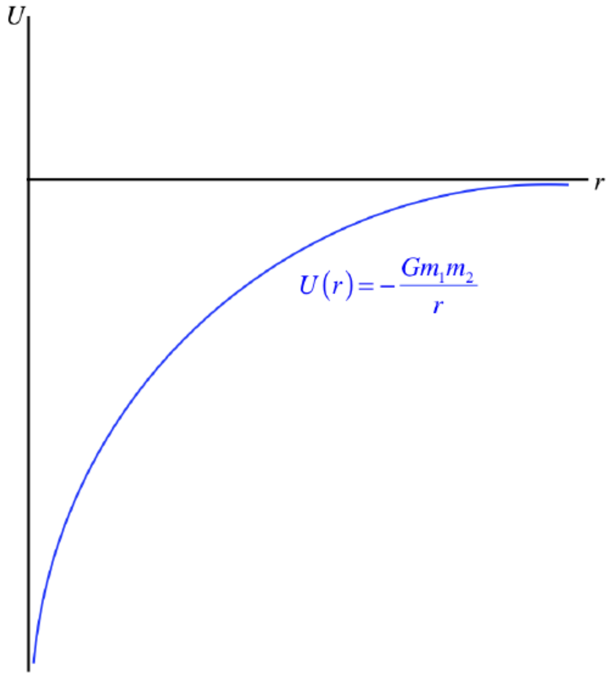

Figure 1.4: Graph illustrating the variation of gravitational potential energy (U) with distance (r)

The origin of binary stars has long been one of the central problems of astronomy. While it is not impossible that some binaries might be created through *gravitational capture* between two single stars, given the very low likelihood of such an event due to potential energy barriers in their self-gravitating systems. The potential energy curve [1.4] typically exhibits a minimum point at a certain separation distance r_min, stars need to overcome this potential energy barrier to get close enough for gravitational capture to occur. At large distances (far from each other), the potential energy is positive and decreases towards zero as stars approach r_min. However, for stars to capture each other gravitationally, they must reach distances where their potential energy is sufficiently negative to facilitate binding, which is typically not achieved in systems involving two isolated stars. Given the high number of binaries currently in existence, this cannot be the primary formation process.

There are several prominent theories of binary and multiple star formation in the literature. The following are the commonly accepted mechanisms (Kratter, 2011).

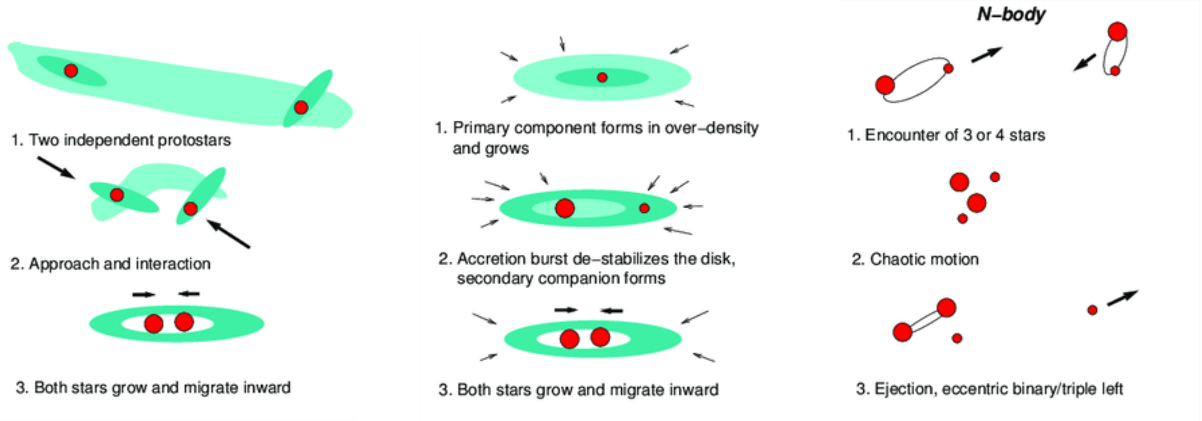
1. Two independent protostars
2. Approach and interaction
3. Both stars grow and migrate inward
1. Primary component forms in over–density and grows
2. Accretion burst de–stabilizes the disk, secondary companion forms
3. Both stars grow and migrate inward
N–body
1. Encounter of 3 or 4 stars
2. Chaotic motion
3. Ejection, eccentric binary/triple left

Figure 1.5: Some commonly accepted binary-star formation mechanisms

1. *Turbulence Fragmentation*: In a turbulent cloud, the non-linear perturbations expected can lead to certain sub-regions within a dense core becoming exceptionally over-dense. These over-dense areas collapse more rapidly than the typical free-fall timescale of the surrounding core material, resulting in the formation of secondary condensations within the core. Alternatively, the turbulence can stretch the gas and dust into filamentary structures, which subsequently fragment into multiple objects. These objects, or proto-stars, then accrete material from their natal core mostly independently. Recent studies by Offner et al (Offner u.a., 2010) have demonstrated that turbulent fragmentation is the predominant mechanism for the formation of binary systems in radiation hydrodynamic simulations of low-mass ($M < M_\odot$) star formation.
2. *Disk Formation*: Models explaining the formation of binary and multiple star systems at a slightly advanced evolutionary stage focus on protostellar disks, which are rotating disks of gas and dust around young newly formed stars. According to the disk fragmentation model (Bonnell, 1994), massive protostellar disks can develop gravitational instabilities. When these disks become unstable, and the gas cools effectively, they can fragment, forming one or more companions in the same plane (coplanar) that accrete from the parent disk and potentially from the primary star's natal cloud, depending on the formation period. When disks are more massive and undergo continuous accretion, simulations suggest that fragmentation may be more common. In this case, secondaries are formed in the disk and quickly accrete to match the primary's mass. Observations of more massive disks support this, indicating that disk fragmentation can result in a wide range of mass ratios. This scenario is most relevant for systems with primaries more massive than the Sun, although recent observations of young clusters suggest it might also apply to lower mass systems (Kraus u.a., 2011).
3. *Dynamic Formation*: Recent studies (Bate u.a., 2003) have suggested that star

clusters form through a dynamic process called *competitive accretion*. In this scenario, a turbulent molecular cloud produces numerous clumps of gas, each approximately at the Jeans mass. These clumps interact and compete to gather mass from the surrounding cloud. Within this environment, binary stars can form through various mechanisms, including the disk methods mentioned above, as well as dynamical interactions between three or more bodies. Additionally, dynamical friction between the protostars and background gas is thought to tighten wider binaries. Unlike the scenarios listed above, the stellar system does not accrete from a fixed core but rather migrates around in a collecting cloud.

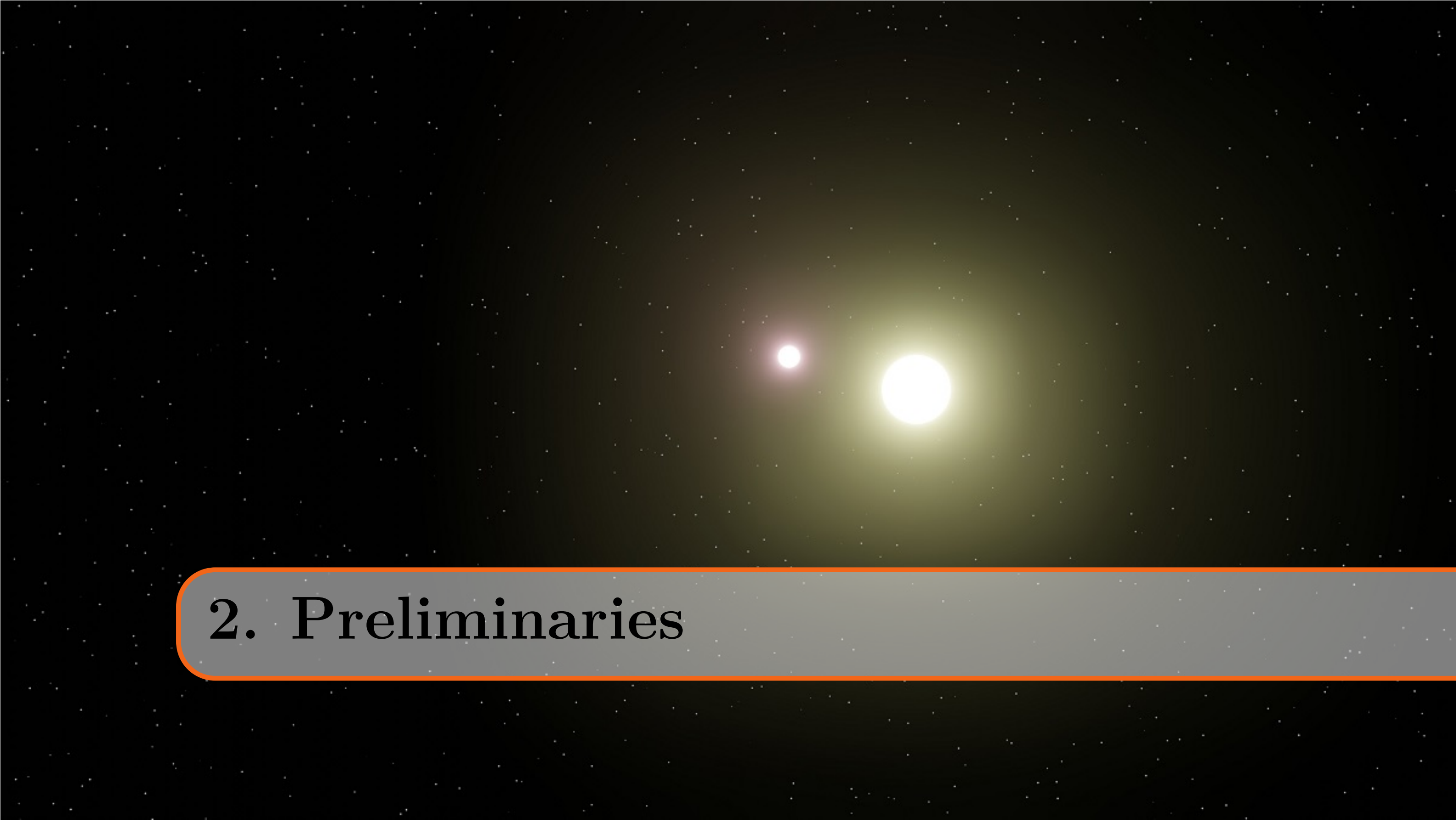

2. Preliminaries

2.1 Celestial Co-ordinates, Celestial Sphere and Epochs

2.1.1 Celestial Co-ordinate

A widely used celestial coordinate system by astronomers is the equatorial coordinate system. Essentially, it is the angular components of the spherical coordinate system centered on Earth with the Earth's rotational axis as the z-axis and the directional location of the sun at the vernal equinox as the x-axis. The angular components are expressed in terms of **Declination** (δ) and **Right Ascension** (α).

The **Declination** (δ) is the equivalent of latitude and ranges from 90° at the north celestial pole to -90° at the south celestial pole. $\delta = 90° - \theta$ where θ is a polar coordinate.

The **Right Ascension** (α) is the equivalent of longitude; due to the rotation of the celestial sphere, it is measured in time (hours, minutes & seconds) you would have to wait from the point that the vernal equinox crosses the meridian until the object of interest crosses the meridian $\alpha = \phi/15°$ where ϕ is a polar coordinate.

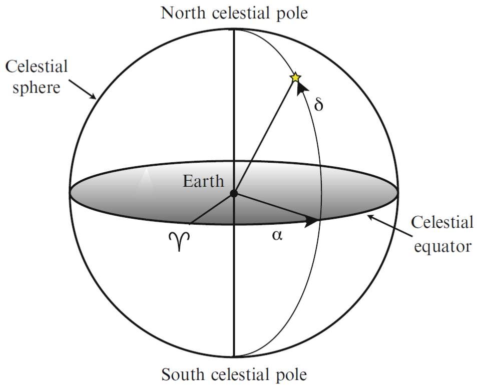

Figure 2.1: Celestial Coordinate

2.1.2 Epochs

Due to precesion the vernal equinox moves at about $50.26''$ /year westward along the ecliptic, and an additional $0.12''$/year due to the earth planet interactions. Therefore, when we give the equatorial coordinates for an object, we must also give the time period for which those coordinates are valid. This time periods are called **Epochs**, which are generally less than about 50 years. For example, Epoch J2000 began on 1st Jan of the year 2000. For taking an observation from a telescope in the correct direction N years after begning of an epoch we need to adjust the coordinates.the correction is linear in N and is given by

$$\Delta\alpha = (m + nsin\alpha tan\delta)N$$

$$\Delta\delta = (ncos\alpha)N$$

where m = 3.075 s/year and n =1.366 s/year = 20.043"/year For J2000.

2.1.3 Celestial Sphere

A consequence of astronomy being an ancient science is that many conventions are derived from old concepts. In this case, all stars are stuck on a sphere called the Celestial Sphere, which surrounds the Earth and rotates around a fixed Earth on a sidereal day. But we now know that is not true and that neither Earth nor the stars are fixed on the Celestial Sphere; instead, the stars themselves move through space.

2.2 Fluxes, Magnitudes, and luminosity

2.2.1 Magnitude

Due to the obvious fact that some stars are brighter than others, a ranking scheme for measuring the brightness of stars was developed in classical times using the human eye as a photon detector. The scale used by **Hipparchus** ranked the brightest stars at the first magnitude ($m = 1$), the dimmest stars that he could see at the sixth magnitude ($m = 6$),Benacquista (2013). In this ranking scheme, brighter stars have lower magnitudes, resulting in the brightest objects now having negative magnitudes. The magnitude scale is based on the human eye, which is logarithmic and could be well approximated where a difference of five magnitudes corresponded to a factor of 100 in brightness.

2.2.2 Radiant flux and luminosity

Radiant flux is the amount of light energy deposited per unit area per unit time.If we define the radiant flux (I) and magnitude for star 1 as I_1 and m_1 and for star 2 as $I_2$and m_2, then

$$\frac{I_2}{I_1} = 100^{(m_1-m_2)/5}$$

The **luminosity** (L) of an object is the total radiated power. We can relate the radiant flux to the luminosity and distance by the inverse square law of light

$$I = \frac{L}{4\pi d^2}$$

2.2.3 Absolute magnitude

In the magnitude scale, no consideration of the distance to the star is taken, resulting in two identical stars having different magnitudes if they are at different distances; therefore

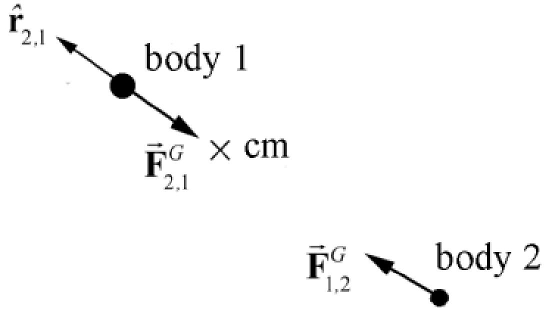

(a) Gravitational force b/w two bodies

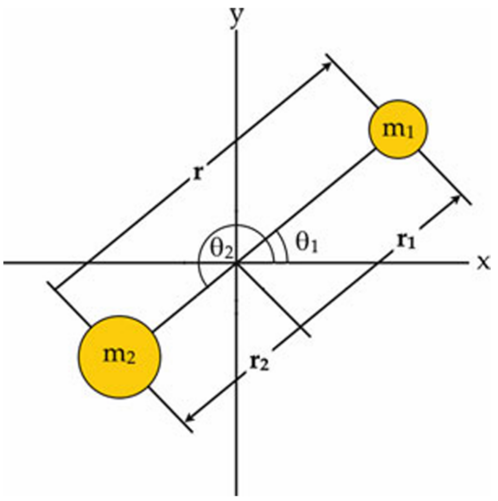

(b) Barycentric co-ordinate system

We define the **Absolute magnitude** (M) to be the magnitude (m) that the star would have if it were placed at a standard distance away, which is 10 parsecs, then

$$M = m - 5log(\frac{d}{10\ pc})$$

2.2.4 Distance modulus(μ)

$$\mu = m - M = 5[log_{10}(d) - 1]$$

The **Distance modulus** (μ) is constant for a cluster of stars that are all at roughly the same distance and thus can be added to each measured magnitude to obtain the absolute magnitudes.

2.3 The 2-Body Problem

We shall determine the equation of motion for the motions of two bodies interacting via a gravitational force (two-body problem) using the force method.

2.3.1 Reducing the Two-Body Problem into a One-Body Problem

The motion of two bodies interacting via gravitational force can be modelled as a single body acted upon by an external gravitational force, with the mass of that single body equal to *the reduced mass*, μ

$$\mu = \frac{m_1 m_2}{m_1 + m_2} \tag{2.1}$$

- **We will solve for the motion of this reduced body and later using the results, derive the motion for individual bodies.**

We begin by considering the binary star in a Barycentric co-ordinate system, i.e., the Center of Mass frame of reference[2.2b]. Here,

$$m_1\vec{r_1} + m_2\vec{r_2} = 0$$

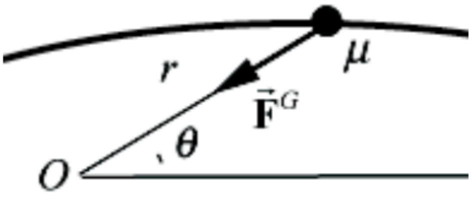

Figure 2.3: Co-ordinate system for orbit of single body

and therefore,

$$m_1 r_1 = m_2 r_2$$

Since the relative separation, $\vec{r} = \vec{r_1} - \vec{r_2}$,

$$\vec{r_1} = \frac{m_2}{M}\vec{r} \qquad \vec{r_2} = -\frac{m_1}{M}\vec{r} \tag{2.2}$$

where $M = m_1 + m_2$ Now, using Newton's second law individually for the two bodies,

$$\vec{F_{2,1}} = m_1 \frac{d^2\vec{r_1}}{dt^2} \quad ; \quad \vec{F_{1,2}} = m_2 \frac{d^2\vec{r_2}}{dt^2}$$

Dividing by the respective masses and subtracting the two equations,

$$\frac{\vec{F_{2,1}}}{m_1} - \frac{\vec{F_{1,2}}}{m_2} = \frac{d^2\vec{r_1}}{dt^2} - \frac{d^2\vec{r_2}}{dt^2} = \frac{d^2\vec{r}}{dt^2}$$

Using Newton's third law,

$$\vec{F_{2,1}} \frac{m_1 + m_2}{m_1 m_2} = \frac{d^2\vec{r}}{dt^2}$$

i.e.,

$$\vec{F_{2,1}} = \mu \frac{d^2\vec{r}}{dt^2} \tag{2.3}$$

We can interpret this result as if there is a **single body of mass** μ with position vector $\vec{r}$ w.r.t. origin. We will now define an $r - \theta$ co-ordinate system to describe the motion of this single body[2.2a][2.2b]. First we will find the distance from the origin, r, as a function of the angle from the x-axis in the counterclockwise direction, θ, i.e., $r(\theta)$. Later on, we will find $r(t)$ and $\theta(t)$.
Now, the constants in this motion are:

- **Total Energy (C):** Since the gravitational force is an internal conservative force, the total energy of the system remains constant.
  Since force is conservative, the potential energy (assuming $U(\infty) = 0$ is given by

$$U(r) = -\frac{Gm_1 m_2}{r}$$

Since we are working in the COM frame[2.2b], the kinetic energy is given in terms of the relative speed, v, of the two bodies.

$$\vec{v} = \frac{d\vec{r}}{dt} = \frac{dr}{dt}\hat{r} + r\frac{d\theta}{dt}\hat{\theta}$$

where $\theta = \theta_1 = \theta_2 - \pi$. Thus, the total energy is given as

$$C = \frac{1}{2}\mu v^2 + U(r)$$

$$\implies \frac{1}{2}\mu\left(\frac{dr}{dt}\right)^2 + \frac{1}{2}\mu r^2\left(\frac{d\theta}{dt}\right)^2 - \frac{G\mu M}{r} = C \tag{2.4}$$

- **Angular Momentum (J):** The angular momentum is constant about the origin as the only force acting is itself directed towards the origin, and hence the net-torque on the system is zero. The angular momentum w.r.t. the origin is given by

$$\vec{J} = \vec{r} \times \mu\vec{v} = r\hat{r} \times \mu(v_r\hat{r} + v_\theta\hat{\theta}) = \mu r v_\theta \hat{k}$$

$$J = \mu r^2\frac{d\theta}{dt} \tag{2.5}$$

We can re-write the equation for total energy as

$$C = \frac{1}{2}\mu\left(\frac{dr}{dt}\right)^2 + \frac{1}{2}\frac{J^2}{\mu r^2} - \frac{G\mu M}{r} \qquad \because \frac{d\theta}{dt} = \frac{J}{\mu r^2} \tag{2.6}$$

2.3.2 Determining the orbital shape, $r(\theta)$

We will do some clever substitutions in Eq. (2.6) as follows:

$$C = \frac{1}{2}\mu\left(\frac{dr}{dt}\right)^2 + \frac{1}{2}\frac{J^2}{\mu r^2} - \frac{G\mu M}{r}$$

- First substitution:

$$u = \frac{1}{r} \tag{2.7}$$

$$\begin{aligned}\implies \frac{dr}{dt} &= \frac{-1}{u^2}\frac{du}{dt} \\ &= -r^2\frac{du}{d\theta}\frac{d\theta}{dt} \\ &= \frac{-J}{\mu}\frac{du}{d\theta} \qquad \because J = \mu r^2\frac{d\theta}{dt}\end{aligned}$$

Thus, the equation becomes

$$\frac{J^2}{2\mu}\left(\frac{du}{d\theta}\right)^2 + \frac{J^2}{2\mu}u^2 - G\mu M u = C$$

- Second substitution:

$$l = \frac{J^2}{G\mu^2 M} \tag{2.8}$$

which implies $\frac{J^2}{\mu} = GM\mu l$. Substituting $\frac{J^2}{\mu}$ into the equation, dividing by $\frac{GM\mu}{2l}$ and adding 1 to both sides, we get

$$l^2\left(\frac{du}{d\theta}\right)^2 + l^2u^2 - 2lu + 1 = \frac{2Cl}{GM\mu} + 1$$

- Third substitution:

$$e^2 = \frac{2Cl}{GM\mu} + 1 \tag{2.9}$$

- And the final substitution:

$$\sigma = lu - 1 \tag{2.10}$$

Thus our equation finally becomes

$$\left(\frac{d\sigma}{d\theta}\right)^2 + \sigma^2 = e^2$$

$$\implies \frac{d\sigma}{d\theta} = \sqrt{e^2 - \sigma^2}$$

Integrating within limits,

$$\int_{\sigma_0}^{\sigma} \frac{d\sigma}{\sqrt{e^2 - \sigma^2}} = \int_{\theta_0}^{\theta} d\theta$$

$$\arcsin\left(\frac{\sigma}{e}\right) - \arcsin\left(\frac{\sigma_0}{e}\right) = \theta - \theta_0$$

We can observe that $|\sigma| \le |e|$ in order for the arcsin to make any sense. We also define $\theta_0 = 0$ and require $\sigma_0 = \sigma(0) = e$ to obtain

$$\arcsin\left(\frac{\sigma}{e}\right) - \arcsin(1) = \theta - 0$$

$$\implies \frac{\sigma}{e} = \sin(\theta + \pi/2) = \cos(\theta)$$

$$\sigma = e\cos\theta \tag{2.11}$$

Reversing all substitutions,

$$r = \frac{l}{1 + e\cos\theta} \tag{2.12}$$

This result Eq. (2.12) is called the ***orbit equation*** for the reduced body, where

$$l = \frac{J^2}{G\mu^2 M} \quad , \quad e = \sqrt{\frac{2Cl}{GM\mu} + 1}$$

We can express the constant quantities, J and C in terms of the described constants as

$$J = \sqrt{\mu^2 GMl} \tag{2.13}$$

$$C = \frac{G\mu M(e^2-1)}{2l} \tag{2.14}$$

The orbit equation as given in Eq. (2.12) is a general conic section and is perhaps somewhat more familiar in Cartesian coordinates.
Let $x = r\cos\theta$ and $y = r\sin\theta$, with $r = \sqrt{x^2+y^2}$. The orbit equation can be written as

$$r = l - er\cos\theta$$
$$\implies \sqrt{x^2+y^2} = l - ex$$

Squaring and rearranging the terms, we get a general expression for a conic section with axis as the x-axis,

$$x^2(1-e^2) + 2exl + y^2 = l^2 \tag{2.15}$$

where e **is the eccentricity of the conic** and l **is the semi-latus rectum of the conic**. Based on different values of eccentricity (or we can say **based on the different values of the two constants, Angular momentum (J) and the Total Energy (C)**), the orbits can be in the following four shapes:

Circular Orbit
When
- $e = 0$
- This implies the total energy, $C = -\frac{Gm_1m_2}{2l} < 0$.

In this case, the equation for the orbit becomes

$$x^2 + y^2 = l^2 \tag{2.16}$$

where l is the radius of the circular orbit. The radius $l = r_0$ in this case and the energy $C = \frac{G\mu M}{2r_0} = C_{min}$.

Elliptical Orbit
When
- $0 < e < 1$
- This implies the total energy, $C_{min} < C < 0$.

In this case the equation for the orbit becomes

$$y^2 + Ax^2 - Bx = k \tag{2.17}$$

where $A, k > 0$. This equation can be reduced to the standard equation for ellipse (Appendix C of (Anchordoqui))

Parabolic Orbit
When
- $e = 1$
- This implies the total energy, $C = 0$.

In this case the equation for the orbit becomes

$$x = \frac{y^2}{2r_0} - \frac{r_0}{2} \tag{2.18}$$

This is the equation of a standard parabola.

Hyperbolic Orbit
When

- $e > 1$
- This implies the total energy, $C > 0$.

In this case the equation for the orbit becomes

$$y^2 - Ax^2 - Bx = k \tag{2.19}$$

where $A, k > 0$. This is the equation of a standard hyperbola.

Summarising the four cases, we have:

Orbit Type	**Eccentricity** (e)	**Total Energy** (C)	**Equation**
Circular	$e = 0$	$C = C_{min} = -\frac{Gm_1m_2}{2l} < 0$	$x^2 + y^2 = l^2 = r_0^2$
Elliptical	$0 < e < 1$	$C_{min} < C < 0$	$y^2 + Ax^2 - Bx = k$
Parabolic	$e = 1$	$C = 0$	$x = \frac{y^2}{2r_0} - \frac{r_0}{2}$
Hyperbolic	$e > 1$	$C > 0$	$y^2 - Ax^2 - Bx = k$

Table 2.1: Characteristics and Equations of Different Orbital Types

2.4 Using the 1-body analysis to solve the original 2-body problem

Referring to Eq. (2.2), we can say that

$$r_1 = \frac{\mu}{m_1} r \qquad \text{and} \qquad r_2 = \frac{\mu}{m_2} r$$

Thus, using Eq. (2.12), we can say that

$$r_1 = \frac{\mu l / m_1}{1 + e\cos\theta}$$

$$r_2 = \frac{\mu l / m_2}{1 + e\cos\theta}$$

Defining $l_1 = \frac{\mu}{m_1} l$ and $l_2 = \frac{\mu}{m_2} l$, we can see that the following equations

$$r_1 = \frac{l_1}{1 + e\cos\theta} \qquad\qquad r_2 = \frac{l_2}{1 + e\cos\theta} \tag{2.20}$$

are similar to Eq. (2.12), with only the latus-recta of respective masses' orbits multiplied by a factor of $\frac{\mu}{m_i}$ and eccentricity remaining the same.
Thus we can say that the orbits of individual bodies are also similar to the hypothetical 1-body case with the origin being at the center of mass of the system and the latus-rectum (l) changed by a factor of $\frac{\mu}{m_i}$.

2.5 Kepler Laws and Elliptical Orbits

2.5.1 Kepler's Laws

Kepler's laws of planetary motion describe the motion of planets around the sun. These laws were formulated by Johannes Kepler in the early 17th century based on the observations of Tycho Brahe. The three laws are:

1. **Kepler's First Law - The Law of Orbits**: All planets move about the Sun in elliptical orbits, with the Sun at one of the foci. The point at which the planet is closest to the Sun is called perihelion, and the point at which it is farthest is called aphelion.
2. **Kepler's Second Law - The Law of Equal Areas**: The radius vector drawn from the Sun to a planet sweeps out equal areas in equal lengths of time. This means that the planet moves faster when it is closer to the Sun and slower when it is farther away.
3. **Kepler's Third Law - The Law of Periods**: The square of the time period of a planet's revolution around the Sun is directly proportional to the cube of its semi-major axis. This means that the orbital period of a planet is longer for orbits with larger semi-major axes.

2.5.2 Properties of elliptical orbits and orbital elements

An elliptical orbit is a Kepler orbit with an eccentricity of less than 1. It is characterized by several key properties:

1. **Eccentricity**: The eccentricity of an elliptical orbit is less than 1, which means that the orbit is not a perfect circle but is rather an oval shape. The eccentricity is a measure of how much the orbit deviates from a circle.
2. **Shape**: The shape of an elliptical orbit is an ellipse, which is a closed curve that is symmetrical about its center. The orbit is stretched out in one direction, resulting in an oval shape.
3. **Energy**: The total energy of an elliptical orbit is negative, which means that the orbit is bound and the object will not escape the gravitational pull of the central body.
4. **Orbital Period**: The time it takes for an object to complete one orbit around the central body is known as the orbital period. For elliptical orbits, the orbital period is related to the semi-major axis of the orbit, and it is longer for orbits with larger semi-major axes.
5. **Velocity**: The velocity of an object in an elliptical orbit varies as it moves along the orbit. The velocity is highest at the point closest to the central body (perihelion) and lowest at the point farthest from the central body (aphelion).
6. **Focus**: In an elliptical orbit, the central body is located at one of the foci of the ellipse. The other focus is empty, and the object moves along the ellipse with the central body at one of the foci.
7. **Angular Momentum**: The angular momentum of an elliptical orbit is constant, which means that the product of the object's mass, velocity, and distance from the central body remains constant throughout the orbit.
8. **Orbital Elements**: The state of an elliptical orbit can be described using six orbital elements: semi-major axis, eccentricity, inclination, longitude of the ascending node, argument of periapsis, and mean anomaly. These elements define the shape and orientation of the orbit.

These properties are crucial in understanding the behavior of objects in elliptical orbits.

The Orbital Elements
Observed binaries do not lie in the plane of the sky, so we need to describe the orientation of the binary using the *orbital elements*. These are defined in terms of both the total angular momentum vector **J** and the total energy of the orbit. The orientation of the binary can be described in terms of the direction of the total angular momentum vector and the direction of the periastron, which give the z- and x-axes in the orbital plane, respectively. These directions are measured relative to a coordinate system that is defined by the tangent plane to the celestial sphere at the location of the binary. A Cartesian coordinate system is defined in terms of the line of sight to the binary from the observer and the tangent to a great circle joining the binary to the north celestial pole. The angle of inclination is defined as the angle between the plane of the orbit and the tangent plane to the celestial sphere. The ascending node (N) is the line defined by the intersection of the plane of the orbit and the tangent plane and points in the direction where the binary passes from *inside* the celestial sphere to *outside* the celestial sphere. Figure 2.4 shows the orientation of the orbit relative to the tangent plane and the three angles that define this orientation. These three angles are -

- **Angle of Inclination** i
- **Longitude of the ascending node** Ω
- **Longitude of the periastron** ω

The shape of the orbit is then given by three quantities:

- **Semimajor Axis** a
- **Eccentricity** e
- **Time of Periastron** T

These six quantities are called the orbital elements. If the orbital elements can be measured, then the masses of the binary can be determined. The orbit will always appear to be an ellipse when viewed on the sky, but unless $i = 0$, the center of mass of the system will not lie at the focus of this apparent ellipse. The angular momentum and total energy are also related to the orbital period and orbital shape. To obtain these relations we begin by noting that the kinetic energy is

$$K = \frac{1}{2}m_1v_1^2 + \frac{1}{2}m_2{v_2}^2 = \frac{1}{2}\mu v^2$$

where $v^2 = \dot{r}^2 + r^2\dot{\theta}^2$ and r and θ are relative separation variables. Now, using $r = l/(1 + e\cos\theta)$, we find that

$$\dot{r} = \dot{\theta}\frac{r^2}{\ell}e\sin\theta = \frac{L}{\ell}e\sin\theta$$

and

$$r\dot{\theta} = \frac{r^2\dot{\theta}}{r} = \frac{L}{r} = \frac{L}{\ell}(1 + e\cos\theta)$$

. From here we get

$$\begin{aligned}
v^2 &= \left(\frac{L}{\ell}\right)^2 \left[e^2\sin^2\theta + 1 + 2e\cos\theta + e^2\cos^2\theta\right] \\
&= \left(\frac{L}{\ell}\right)^2 \left[e^2 + 1 + 2e\cos\theta\right] = \left(\frac{L}{\ell}\right)^2 \left[2(1+\cos\theta) - 1 + e^2\right] \\
&= \left(\frac{L}{\ell}\right)^2 \left[\frac{2\ell}{r} - (1-e^2)\right] = \left(\frac{L^2}{\ell}\right)\left[\frac{\ell}{r} - \frac{1-e^2}{\ell}\right] \\
&= \left(\frac{L^2}{\ell}\right)\left[\frac{2}{r} - \frac{1}{a}\right]
\end{aligned}$$

where we have used $a = l(1-e^2)$ in the last step. Now from Kepler's second law, we have $L = 2\pi ab/P$, where P is the orbital period. Noting that $b^2 = a^2(1-e^2)$ we find

$$\begin{aligned}
L &= \frac{4\pi^2 a^2 b^2}{P^2} = \frac{4\pi^2 a^3}{P} a(1-e^2) \\
&= GMa(1-e^2) \\
&= GM\ell
\end{aligned}$$

where we have used Kepler's third law. Finally we have

$$v^2 = GM\left[\frac{2}{r} - \frac{1}{a}\right]$$

and so the kinetic energy is

$$\begin{aligned}
K = \frac{1}{2}\mu v^2 &= \frac{1}{2}\frac{m_1 m_2}{M} GM\left[\frac{2}{r} - \frac{1}{a}\right] \\
&= \frac{Gm_1m_2}{r} - \frac{Gm_1m_2}{2a}
\end{aligned}$$

Now, the potential energy is $\Omega = -Gm_1m_2/r$, so the total energy is

$$C = K + \Omega = -\frac{Gm_1m_2}{2a}$$

The total angular momentum is $J = m_1L_1 + m_2L_2$, where

$$\begin{aligned}
L_1 &= \frac{m_2^2}{M^2} L \\
L_2 &= \frac{m_1^2}{M^2} L \\
L^2 &= GMa(1-e^2)
\end{aligned}$$

This gives:

$$\begin{aligned}
J &= \frac{1}{M^2}(m_1m_2^2 + m_2m_1^2)\sqrt{GMa(1-e^2)} \\
&= m_1m_2\sqrt{\frac{Ga(1-e^2)}{M}} \\
&= \frac{2\pi}{P}\frac{m_1m_2a^2\sqrt{1-e^2}}{M}
\end{aligned}$$

Thus the total energy is fixed by the masses and the semimajor axis, while the total angular momentum also depends upon the period and the eccentricity.

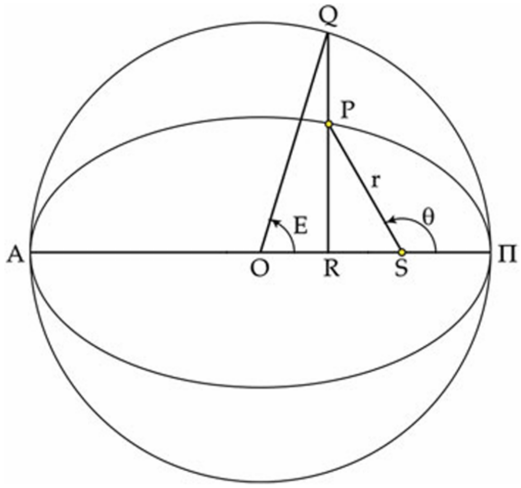

Figure 2.4: Derivation of the eccentric angle time-dependence

2.5.3 Motion of the star system with time

To derive the time-dependence of the eccentric anomaly, E, as shown in the figure Fig. (2.4) (where θ is the true anomaly), we use the geometry of ellipse.
Applying trigonometry in ΔPRS in Fig. (2.4)

$$PR = r\sin\theta$$

Also since $PR = a\sqrt{1-e^2}\sin E$ (co-ordinate geometry of ellipse),

$$\sin\theta = \frac{\sqrt{1-e^2}}{1-e\cos E}\sin E \tag{2.21}$$

Differentiating w.r.t. E,

$$\cos\theta\,\frac{d\theta}{dE} = \sqrt{1-e^2}\,\frac{cosE - e}{(1-e\cos E)^2}$$

Now, since $r\cos\theta = -RS = OS - OR$,

$$r\cos\theta = a\cos E - ae$$

Substituting the value of $\cos\theta$ from here into the equation,

$$\frac{d\theta}{dE} = \frac{\sqrt{1-e^2}}{1-e\cos E}$$

Also, $d\theta = \frac{J}{\mu r^2}dt$ from Eq. (2.5), substituting $d\theta$ and integrating,

$$\int_T^t \frac{J}{\mu a^2\sqrt{1-e^2}}\,dt = \int_0^E (1-e\cos E)\,dE$$

Thus,

$$E - e\sin E = \frac{L}{ab}(t-T) \tag{2.22}$$

where T = time when the body passes through periastron, L = specific angular momentum $\left(\frac{J}{\mu}\right)$, b = semi-minor axis. Also,

$$r^2 d\theta = L dt$$

$$\int_0^{2\pi} r^2 d\theta = L \int_T^{T+P} dt \qquad \text{,where } P \text{ is the period of revolution}$$

$$2\pi ab = LP$$

Thus,

$$\frac{L}{ab} = \frac{2\pi}{P} = \omega \tag{2.23}$$

Hence we can alternatively write Eq. (2.22) as

$$E - e \sin E = \frac{2\pi}{P}(t - T) \tag{2.24}$$

We can compute the value of E at any given point of time, with the help of orbital parameters.
Also, using Pythagoras theorem in right angled ΔPRS, we get

$$r = a(1 - e \cos E) \tag{2.25}$$

And, we have Eq. (2.21) as a relation of θ in E.
Thus, using computational methods, we can caculate r and θ at any time t. And as discussed in section (2.4), we can use the results to determine the required values for individual bodies.

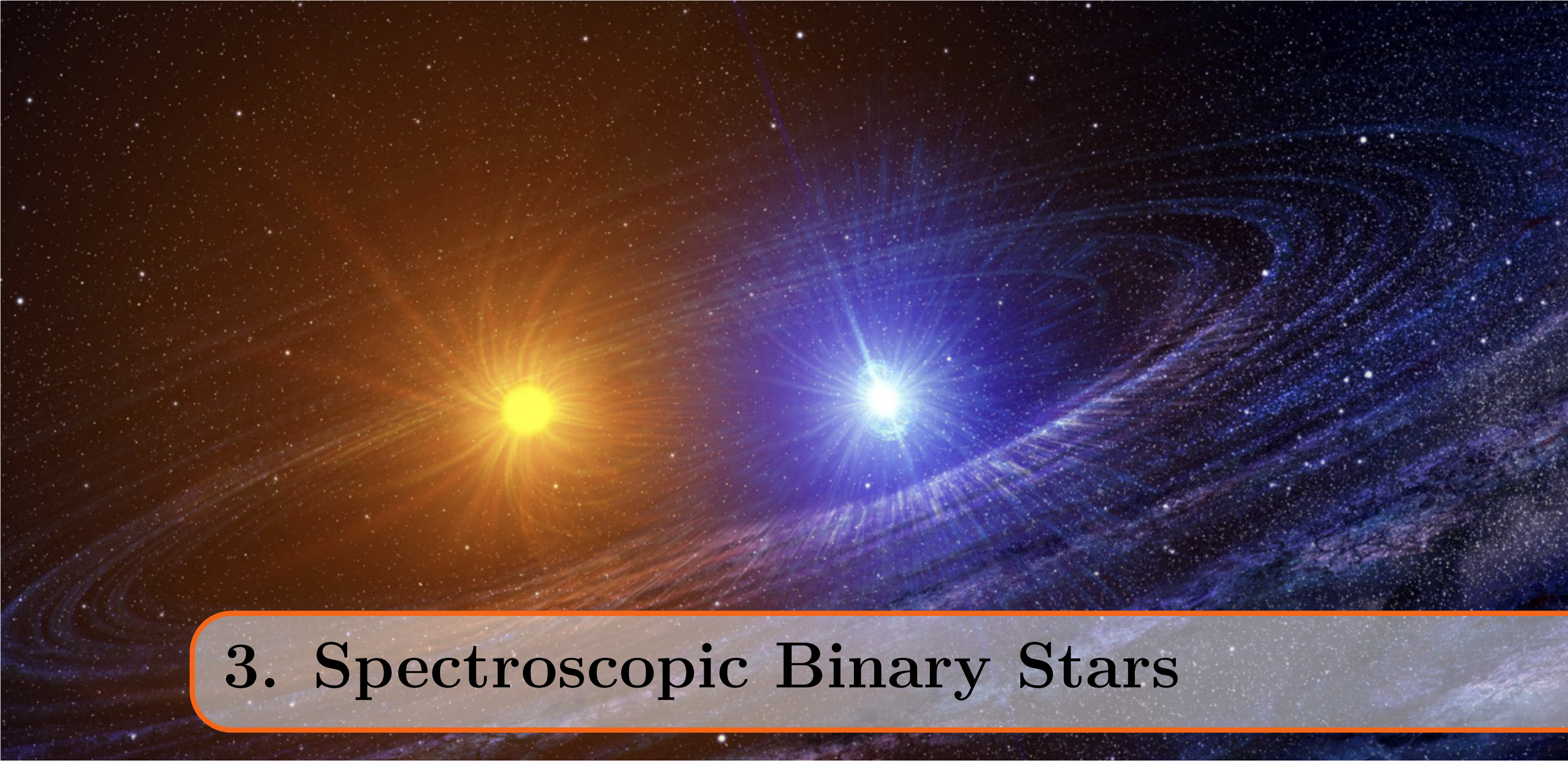

3. Spectroscopic Binary Stars

So far we have seen some of the basics and motivations[1] behind studying binaries in Chapter 1 and discussed celestial mechanics in detail (Ch. 2). Of the three classes of binary stars discussed in Ch. 1: *astrometric*, *spectroscopic* and *eclipsing*, we will give a detailed overview of **spectroscopic binaries** in this chapter.

3.1 Introduction

The first *visual binary* to be discovered was *Mizar* (ζ U Ma) and the discovery is often attributed to the Italian astronomer J. B. Riccioli who discovered it in around 1650 (Burnham, 1978). However, its earliest records can be found in the letter of Castelli to Galileo, and Galileo's own record of it dated post Castelli's letter (Mamajek u.a., 2010; Siebert, 2005). *Astrometric/visual binaries* are great laboratories for scientists. However, when the component stars of a binary system are close enough to not be spatially resolved, we need some other pathways to study the binaries. One such pathway is offered by studying the periodic movements of the spectral lines or the radial velocity curves. Interestingly, one of the components of *Mizar* (ζ U Ma) was also the first one to be discovered in a binary using this technique. It was discovered by E. C. Pickering at the dusk of the nineteenth century. However, three months after its discovery, H. C. Vogel found that *Algol* (first eclipsing binary discovered in 1782 by Goodericke) was also a spectroscopic binary (Batten, 1989). These binary systems are useful in measuring the *multiplicity fraction* of the stars which varies as a function of age, mass and chemical composition of the stars. This can be further used to probe star formation processes (Merle, 2024; Duchêne u.a., 2013). The multiplicity rate and the distribution of the orbital period are steep functions of the primary mass and the mass ratio distribution is flat for most populations except for the lowest mass objects. Stellar multiplicity is a direct outcome of the star-formation process and its trends can be compared to numerical and analytical models of star formation. This shall allow us to refine our understanding of the physical processes in star formation.

---

[1] Also see (Southworth, 2020, 2012) for more details.

As the name suggests, spectroscopic binaries are studied using their spectra (Benacquista, 2013). Based on the observation of spectral data from a binary system, how can one deduce that the spectra is from a binary system? We observe the spectra of a single system over extended periods, known as long cadence observations. Each spectrum is fitted, and significant lines, such as hydrogen and metal lines, are identified. Once these lines are identified, we calculate their redshift or radial velocity. This process is repeated for all spectra obtained during the long cadence period, which may span several days. We then plot the radial velocity against time to examine the variability of the curve. If the curve exhibits periodic variations, this indicates the presence of a binary system. Using the periodic change in the wavelength of the two sets of spectrum lines due to the *Doppler effect* over a sufficient period of time, some of the orbital characteristics can be thereby extracted from the *radial velocity curve*. It might be possible that one of the components is significantly brighter than the other, in which case, only one spectrum is observable. On this basis, the spectroscopic binaries are classified into *single-lined spectroscopic binaries* (SB1) and *double-lined spectroscopic binaries* (SB2), as discussed in Section 1.2.

Also note that the binary as a whole can have a velocity (referred to as the *systemic velocity* V_γ) towards or away from the Sun. The spectra observations are with respect to the Earth, and not the Sun. So, corrections must be made to the observed radial velocities accounting for the motion of Earth around the Sun as well as around its own axis of rotation.

3.2 The Radial Velocity Curve

3.2.1 Notations and definitions

We will refer to the center of mass of the binary system as C. The plane tangent to the point C on the celestial sphere is referred to as the *plane of the sky*. The inclination angle i is the angle between the *orbital plane* and the *plane of the sky*. It is also equal to the angle between the position vector of C and the *orbital angular momentum* of the binary system. S_1 and S_2 are the two stars of the binary system. We denote the *semi-major axis* of the orbit of S_1 about C as a_1 and the *eccentricity* as e. The semi-latus rectum $l_1 = a_1(1-e^2)$. The *true anomaly* is denoted as θ. The *specific angular momentum*, L_1, of S_1 about C is given $L = r_1^2\dot{\theta} = \sqrt{GMl_1}$, where, r_1 is the distance of S_1 from C, and $M = \frac{m_2^3}{(m_1+m_2)^2}$. The *orbital period*, P, is given by $P^2 = \frac{4\pi^2}{GM}a_1^3$. The mean motion n (average angular speed) is ${}^{2\pi}/{}_{P}$ and thus, $n^2a_1^3 = GM$. We can therefore express the specific angular momentum as

$$L_1 = r_1^2\dot{\theta} = na_1^2\sqrt{1-e^2}. \tag{3.1}$$

We denote the *argument of latitude* as Θ and the *argument of periastron* as ω. It follows that $\Theta = \omega + \theta$. The perpendicular distance of S_1 from the *plane of the sky* is denoted as z_1. β is the angle between r_1 and the line joining C and the point where the perpendicular from S_1 meets the *plane of the sky*. It then follows that

$$\begin{aligned} z_1 &= r_1 sin(\beta) \\ &= r_1 sin(i) sin(\omega + \theta). \end{aligned} \tag{3.2}$$

3.2.2 Radial velocity

The radial velocity V of S_1 relative to the Sun is given by

$$V = V_\gamma + \dot{z} \tag{3.3}$$

where V_γ is the *systemic velocity* and $z = z_1$ as we are considering only one star currently. The equation to ellipse is given by

$$\begin{aligned} r_1 &= \frac{l_1}{1 + ecos(\theta)} \\ &= \frac{a_1(1-e^2)}{1 + ecos(\theta)}. \end{aligned} \tag{3.4}$$

Differentiating Eq. 3.2 and 3.4 and using Eq. 3.1, 3.4, we obtain

$$\frac{\dot{z}}{sin(i)} = \frac{na_1(1+ecos(\theta))}{\sqrt{1-e^2}} \left(\frac{esin(\theta)sin(\omega+\theta)}{1+ecos(\theta)} + cos(\omega+\theta) \right) \tag{3.5}$$

or

$$\frac{\dot{z}}{sin(i)} = \frac{na_1}{\sqrt{1-e^2}} \left(esin(\theta)sin(\omega+\theta) + (1+ecos(\theta))cos(\omega+\theta) \right). \tag{3.6}$$

Note that $(esin(\theta)sin(\omega+\theta) + ecos(\theta)cos(\omega+\theta) = ecos(\omega)$. So,

$$\dot{z} = K_1 \left(cos(\omega+\theta) + ecos(\omega) \right) \tag{3.7}$$

where, $K_1 = \frac{na_1 sin(i)}{\sqrt{1-e^2}}$ and $[K_1] = [\text{speed}]$.

We can now express the *radial velocity* including the *systemic velocity* as a function of *true anomaly* and elements as

$$V = V_\gamma + K_1 \left(cos(\omega+\theta) + ecos(\omega) \right). \tag{3.8}$$

It can be observed that K_1 is the *semi-amplitude of the radial velocity curve.*

Eq. 3.8 gives us RV as a function of *true anomaly* θ and a few other parameters discussed in detail further in Sec. 3.5. From the discussion in Section 2.5.3 it follows that the *true anomaly* θ is related to the *eccentric anomaly* E, as

$$cos(\theta) = \frac{cos(E) - e}{a - ecos(E)} \tag{3.9}$$

We know the time evolution of the *eccentric anomaly* E as

$$E - esin(E) = \frac{2\pi}{P}(t - T) \tag{3.10}$$

where T is the time at periastron passage and $E = 0$ at the periastron. Using trigonometric identities, the following useful expressions follow from the above:

$$sin(\theta) = \frac{sin(E)\sqrt{1-e^2}}{1 - ecos(E)} \tag{3.11}$$

$$tan(\theta) = \frac{sin(E)\sqrt{1-e^2}}{cos(E) - e} \tag{3.12}$$

$$tan\left(\frac{\theta}{2}\right) = \sqrt{\frac{1+e}{1-e}} tan\left(\frac{E}{2}\right) \tag{3.13}$$

In case of double-lined binaries, two radial velocity curves are obtained. They are not quite mirror images of each other as the semi-amplitudes of each of the component stars follows an inverse relation with the mass of the respective star. The *systemic velocity* in these cases is easily obtained, because the two curves cross when the radial velocity of each of the component stars is equal to the radial velocity of the system. Fig. 3.1 shows several RV curves for some SB1 and SB2 systems.

Measuring the radial velocity

But, how do you measure the radial velocity? As we briefly mentioned in Sec. 3.1, this is done by considering the *Doppler effect* on radiations from the source stars. When stars move towards or away from us, the light from them gets blue or red shifted as comapared to a non-moving source with respect to us. We can then compare the spectral lines and get the difference between the observed wavelength and wavelength recorded from non-moving sources for similar lines in the spectra. In the non-relativistic limit, the measured radial velocity can then be simply given as

$$V = c\frac{\Delta\lambda}{\lambda} \tag{3.14}$$

where c is the speed of light, $\Delta\lambda$ is the difference between the wavelength and λ is the laboratory value of the wavelength.

It is quite a common scheme in astronomy to exploit the *Doppler effect* to measure radial velocities and use them for various science cases. (See (Meunier, 2021) for a review of the context of RV observations and their typical properties including the effects of stellar activity, and also (Lovis u.a., 2010; Endl u.a., 2007; Kaushik u.a., 2024) for the science use case of RVs in the context of exoplanets.)

3.3 Extracting parameters from the RV curve

In the previous section we have described the RV curve and derived the equations related to it. In practice, what we observe and directly get from the data are the RV curves. Now, we will see how we can use the RV curve to extract the parameters that describe the binary star systems.

3.3.1 Orbital and Spectroscopic parameters

We have seen in the previous section that $V = V_\gamma + K[cos(\theta+\omega) + ecos(\omega)]$ where $K = \frac{2\pi asin(i)}{P\sqrt{1-e^2}}$ is the *semi-amplitude of the velocity* and V_γ is the radial velocity of the center of mass of the binary system (systemic radial velocity). From this, it follows that

$$V_{\max} = K[ecos(\omega) + 1] + V_\gamma \tag{3.15}$$

$$V_{\min} = K[ecos(\omega) - 1] + V_\gamma. \tag{3.16}$$

This implies

$$K = \frac{1}{2}\left(V_{\max} - V_{\min}\right) \tag{3.17}$$

and

$$ecos(\omega) = \frac{1}{2K}(V_{\max} + V_{\min}) \tag{3.18}$$

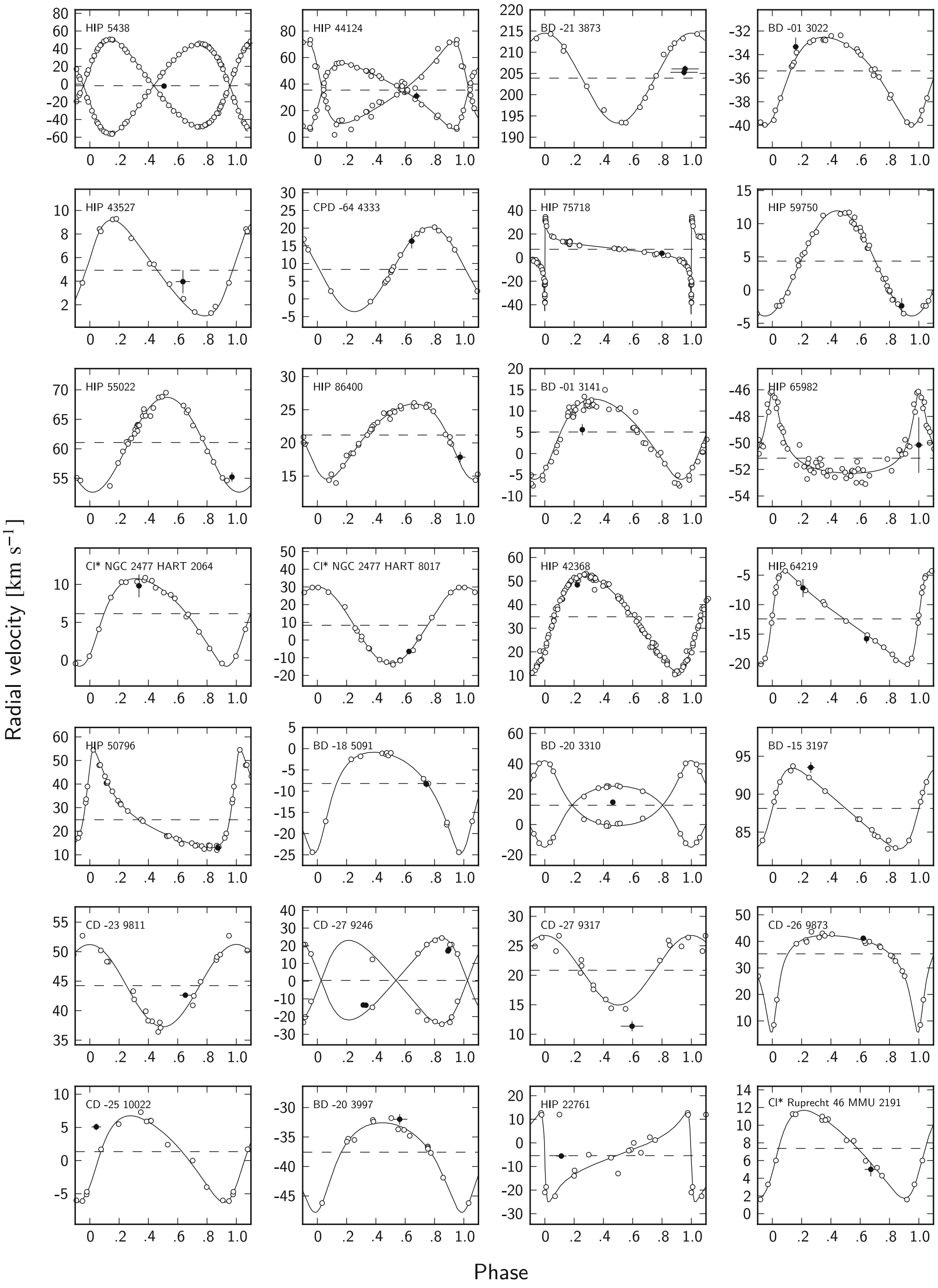

Figure 3.1: Figure 7 from Matijevič u.a. (2011). Various radial velocity curves for several SB1 and SB2 systems.

That is, we can determine K by just measuring the maximum and minimum velocity from the RV curves.

If we observe a double-lined spectroscopic binary, we can determine

$$K_1 = \frac{2\pi a_1 sin(i)}{P\sqrt{1-e^2}} \tag{3.19}$$

$$K_2 = \frac{2\pi a_2 sin(i)}{P\sqrt{1-e^2}} \tag{3.20}$$

along with e, ω and V_γ. It immediately follows that

$$a_1 sin(i) = \frac{\sqrt{1-e^2}}{2\pi} K_1 P \tag{3.21}$$

$$a_2 sin(i) = \frac{\sqrt{1-e^2}}{2\pi} K_2 P. \tag{3.22}$$

As long as we do not know the inclination angle i, we can not escape from the degeneracy between the *semi-major axis* and the *inclination.* We can, however, perform some more jugglery and compute a few other parameters as discussed below.

In the COM frame of reference, $m_1 a_1 = m_2 a_2$ where m_1 and m_2 are the masses of S_1 and S_2, respectively. Also, from Kepler's Third Law, we have $GM = \frac{4\pi^2 a^3}{P^2}$ where $M = \frac{m_2^3}{(m_1+m_2)^2}$. We can express m_2 as

$$m_2 = m_1 \frac{a_1}{a_2} = m_1 \frac{a_1 sin(i)}{a_2 sin(i)} = m_1 \frac{K_1}{K_2}. \tag{3.23}$$

Substituting this in the expression for Kepler's Third Law, we get

$$m_1 sin^3(i) = \frac{P}{2\pi G}(1-e^2)^{\frac{3}{2}}(K_1+K_2)^2 K_2 \tag{3.24}$$

$$m_2 sin^3(i) = \frac{P}{2\pi G}(1-e^2)^{\frac{3}{2}}(K_1+K_2)^2 K_1. \tag{3.25}$$

Hence, in the case of *double-lined spectroscopic binaries* we can obtain the range of masses of the component stars, but the individual masses can not be inferred due to the *mass-inclination* degeneracy until we get the value of *inclination angle.* In the case of *single-lined spectroscopic binaries* we can measure the RV of only one component of the binary. In this case, we cannot get the values of $m_1 sin^3(i)$ and $m_2 sin^3(i)$. However, we can obtain an expression for the *mass-function*, $f(m)$. We can substitute $K_2 = \frac{m_1 K_1}{m_2}$ in the Eq. 3.24 to obtain

$$m_2 sin^3(i) = \frac{PK_1^3}{2\pi G}(1-e^2)^{\frac{3}{2}}\left(\frac{m_1+m_2}{m_2}\right)^2. \tag{3.26}$$

Hence,

$$f(m) = \frac{m_2^3 sin^3(i)}{(m_1+m_2)^2} = \frac{PK_1^3}{2\pi G}(1-e^2)^{\frac{3}{2}}. \tag{3.27}$$

If the system is also an astrometric/visual binary, then we can obtain the value of the *inclination angle i* and remove the degeneracies discussed above.

3.4 Period

Finding the time period from the RV curve could seem very straightforward but there are some subtleties involved. There can be cases where we are recording the data at time intervals which are greater than some multiple of the actual time period. Given enough such observations over a long time period, the RV may be attaining periodic maxima and minima which are not recorded after every actual time period. In that case, one can mistakenly consider the distance between the two peaks in the RV curve as the time period. So, how do we deal with this problem? We first note that this time duration is not equal to the time period but is equal to an integral multiple of the time period, provided the time period remains a constant in that duration.

Suppose that we find the time between two different couple of consecutive maxima are t_1 and t_2. Then, we can say t_1 and t_2 are integral multiples of the actual time period P. Can we do better than this? Yes! $|t_1 - t_2|$ is an integral multiple of P. So, it makes sense to record the measurements at different intervals and not exact regular intervals. That is, $P' = uP$ where $P' = |t_1 - t_2|$ and $u \in \mathbb{N}$. Thus, the data should be recorded at very different time intervals so as to get a number of spurious time periods P'. Given a large number of data points, we can get the actual time period by taking the minima of all the spurious time periods.

Once the actual time period is obtained, we can shift all the data points into one bin of the time period by subtracting some integral multiple of P from the recorded time.

3.5 Refining the orbital elements

We ask the question: *What parameters does the radial velocity depends on?* We recall

$$V = V_\gamma + K_1\left(cos(\omega + \theta) + ecos(\omega)\right).$$

where

$$K_1 = \frac{2\pi a_1 sin(i)}{P\sqrt{1-e^2}}.$$

θ is a function of the time t, and the elements T and e. We can note that the radial velocity V is a function of time t and the orbital elements V_γ, K_1, ω, e, n and T where $n = 2\pi/P$ i.e.

$$V = V(t; V_\gamma, K_1, \omega, e, n, T). \tag{3.28}$$

Consider that we have RV measurement data $\{(V_{\text{obs}}, t)\}$ recorded for different times for a spectroscopic binary system. Now, we wish to get the orbital parameters of the system using this data. For each time of the observation, we can compute the RV value V_{cal} using Eq. 3.8 using the preliminary values. We will choose the least sum of squares scheme and will minimize the sum of residuals i.e. $\sum (V_{\text{obs}} - V_{\text{cal}})^2$ shall be minimized.

We can express the variation in V as

$$\delta V = \frac{\partial V}{\partial V_\gamma}\delta V_\gamma + \frac{\partial V}{\partial K_1}\delta K_1 + \frac{\partial V}{\partial \omega}\delta\omega + \frac{\partial V}{\partial e}\delta e + \frac{\partial V}{\partial n}\delta n + \frac{\partial V}{\partial T}\delta T \tag{3.29}$$

to first order. Substituting the values of the partial derivatives, we get

$$\begin{aligned} \delta V =& \delta V_\gamma + (cos(V+\omega) + ecos(\omega))\delta K_1 - K_1(sin(\theta+\omega) + esin(\omega))\delta\omega \\ & K_1\left(cos(\omega) - \frac{(2+ecos(\theta))sin(\theta+\omega)sin(\theta)}{1-e^2}\right)\delta e \\ & \frac{sin(\theta+\omega)(1+ecos(\theta))^2K_1(t-T)}{(1-e^2)^(3/2)}. \end{aligned} \tag{3.30}$$

If we have six or more measurements, we can get a system of conditional equations and we can keep changing the paramters until we obtain the *improved* set of elements. This job can be best done using a computer.

3.6 Summary

We have seen that spectroscopic binaries allow us to study the binary star systems which may be very close to be resolved as visual binaries. We have described how we can obtain the quantities for spectroscopic binaries listed in Table **??**. Note that we can not obtain any size parameters using spectroscopic binaries. No information about the semi-major axis can be obtained using single-lined spectroscopic binaries (SB1). We can, however, get the projection of the semi-major axis $asin(i)$ in the case of double-lined spectroscopic binaries (SB2). The degeneracy with the inclination can not be resolved using the RV method. This degeneracy also shows up with mass parameters $m_{1,2}sin^3(i)$ (Eq. 3.24 and 3.25) which can be obtained only in the case of SB2. The best we can do in the case of SB1 is to obtain the mass function $f(m)$ (Eq. 3.27).

3.7 Further comments

We have seen that K can be expressed in terms of $V_{\max}$ and $V_{\min}$ (Eq. 3.17). An inspection of Eq. 3.19 and 3.20 makes it clear that the RV method will not be very effective for the face-on cases (i.e. $i = 0, \pi$) as the semi-amplitude of the velocity K will be zero for such cases. Also, K is inversely proportional to the time period P. It is easier to study spectroscopic binaries if they have short orbital periods and high inclination (i.e. $\frac{2i}{\pi} \approx 1$) in order to maximize amplitude of the RV variation. For SB2, the case when $i = \pi/2$ gives us an eclipsing binary which allow us to extract all the parameters including the size parameters given the RV curve. We will see more details about such binaries in Chapter 4.

There are many science-case studies using spectroscopic binaries and the RV method. We mention some of the studies for interested readers. Massive binary evolution is a very active area of research and mass discrepancy is one of the major problems. (Tkachenko, 2015) discusses two massive binary systems, V380 Cyg and σ Sco and testing high-mass stellar evolution models by considering asteroseismic measurements. There have also been studies to obtain precise RV measurements to test, improve and constrain the Keplerian orbital solutions for spectroscopic binary star systems (Heyne u.a., 2020). Studies about collapsed compact objects (like neutron stars) through SB1 have been performed for more than half a century. Such searches of collapsed objects using spectroscopic binary data are described in (Trimble u.a., 1969) and in the more recent (Trimble u.a., 2018). There have also been studies on constraining dark matter fraction inside stars using spectroscopic binaries which is described in (Peled u.a., 2022).

The field is rich with questions that need to be answered. As discussed before, the edge-on cases for SB2 are particularly very interesting and the next chapter is completely dedicated to such cases of eclipsing binaries.

4. Eclipsing Binary Stars

4.1 Introduction

Binary star systems are systems of two stars that orbit around a common center of mass. In some of these binary systems, the orbital plane of the two stars lies so nearly in the line of sight of the observer that the components undergo mutual eclipses (contributors, 2023). These types of binary systems are known as eclipsing binaries.

Eclipsing binaries are characterized by periods of constant light, punctuated by periodic drops in intensity when one star passes in front of the other. The brightness may drop twice during the orbit, once when the secondary star passes in front of the primary star and once when the primary star passes in front of the secondary star (contributors, 2023). The deeper of the two eclipses is called the primary eclipse, regardless of which star is being occulted, and if a shallow second eclipse also occurs it is called the secondary eclipse (contributors, 2023).

Eclipsing binaries are important astrophysical objects as they allow astronomers to determine the masses, radii, and other physical properties of the component stars through careful analysis of the light curves and other observational data (contributors, 2023). They also provide insights into the formation and evolution of binary star systems, which are common in our galaxy.

The first ever observed eclipsing binary was Algol, a triple star system in the constellation Perseus, which was discovered in 1667. Algol is the best-known example of an eclipsing binary and has been extensively studied due to its unique properties (contributors, 2023).

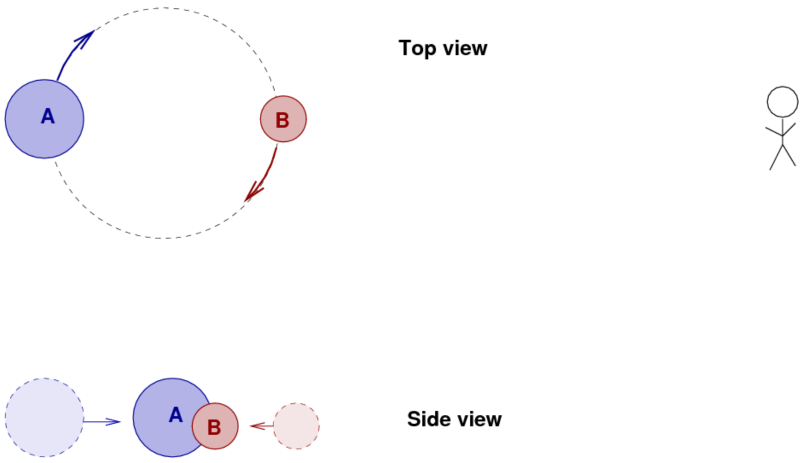

Figure 4.1: A Representation of different views of a Binary System

4.1.1 Types of Eclipsing Binaries

Eclipsing binaries can be classified based on the relative sizes and separations of their component stars. Because not all the Binaries acts like same, which is proved by Light Curves of Binaries. So what makes them different?

So depending on the intimacy of their dance, these stellar couples exhibit distinct characteristics. This journey delves into three primary types of eclipsing binaries, each showcasing a different level of stellar interaction: detached, semi-detached, and contact binaries. By exploring their unique properties, we unlock the secrets hidden within their eclipses, unveiling the fascinating story of stellar evolution and the intricate dynamics of binary systems. So here is the classification:-

- **Detached :** Well-separated stars with minimal interaction. Light curve shows a sharp U-shaped dip during eclipse. If we talk about historical evidence Algol is the first ever Eclipsing Binary system ever observed by Babylonian in about 1300BC. Examples: Algol etc.

- **Semi-detached :** One star fills its Roche lobe, transferring mass. The light curve exhibits an asymmetrical dip. Examples: Beta Lyrae etc.

- **Overcontact :** Close binary with tidally distorted stars, potentially sharing a common atmosphere. The light curve shows a shallow, rounded dip. Examples: W Ursae Majoris etc.

4.1.2 Some important Space Missions About Eclipsing Binares

1. **Kepler**
    - **Mission:** Launched in 2009, Kepler primarily aimed to detect exoplanets transiting their host stars.
    - **Eclipsing Binary Detection:** Due to its high-precision, long-duration observations (months to years), Kepler identified a significant number of eclipsing

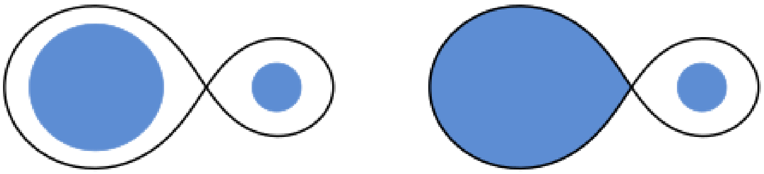

(a) Detached Binary (b) Semi-detached Binary

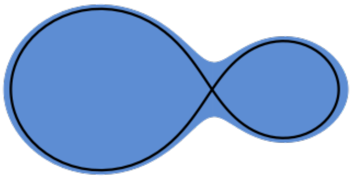

(c) Contact Binary

Figure 4.2: Schematic illustrations of stellar binary systems: (a) detached, (b) semi-detached, and (c) contact. In a detached binary, the stars are gravitationally bound but don't share a common atmosphere. In a semi-detached binary, one star fills its Roche lobe and transfers mass to the other. In a contact binary, both stars fill their Roche lobes and share a common envelope.

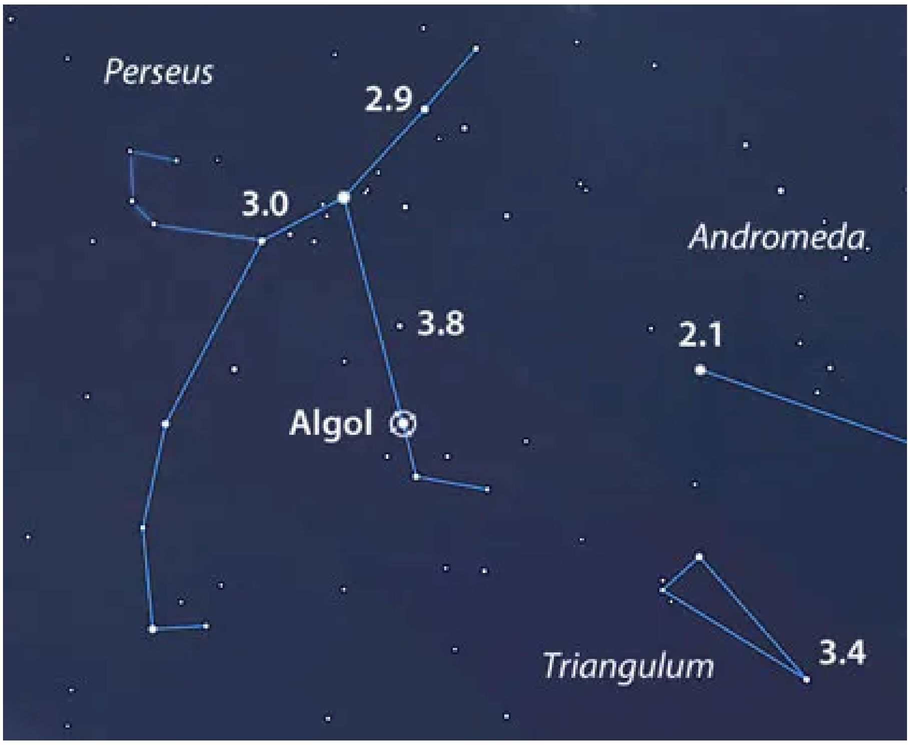

Figure 4.3: Algol,the first ever observed eclipsing binary

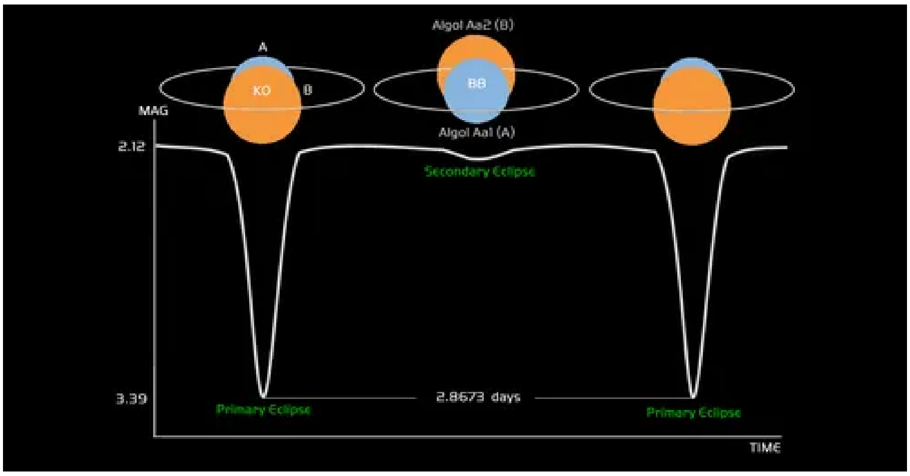

Figure 4.4: Dimming Algol

Figure 4.5: The NASA Kepler Mission

binaries. These detections were often serendipitous - stars that weren't initially targeted for exoplanet searches exhibited periodic dimming due to eclipses.

- **Impact:** Kepler's data provided a wealth of information on EB properties like orbital periods, relative sizes, and mass ratios. This data has been crucial for calibrating stellar models and understanding binary interactions.

2. **Tess**
   - **Mission:** Launched in 2018.TESS is the successor to Kepler, focusing on shorter timeframes (days to weeks) and a much larger sky area.
   - **Eclipsing Binary Detection:** Similar to Kepler, TESS detects EBs as periodic dips in the light curves of stars. However, its shorter observation windows are better suited for identifying short-period eclipsing binaries that Kepler might have missed.
   - **Impact:** TESS is expected to discover a large number of short-period EBs, including those containing compact objects like neutron stars or white dwarfs. This data will be valuable for studying binary evolution and the formation of exotic objects.

Figure 4.6: The NASA TESS mission

4.2 Astrophysical Significance

Eclipsing binaries aren't just celestial light shows; they're powerful tools that have revolutionized our understanding of stars. Here's how these cosmic duos act as game-changers in stellar astrophysics:

1. **Stellar Forensics:** Eclipsing binaries allow us to measure a star's mass, radius, temperature, and luminosity with incredible precision – better than 1-2%! This high accuracy is crucial for testing and refining stellar evolution models, essentially giving us a roadmap for how stars live and die.
2. **Cosmic Laboratories:** Forget Bunsen burners, eclipsing binaries are nature's laboratories! They offer a front-row seat to observe various stellar phenomena. From the internal vibrations of stars (asteroseismology) to the dynamic interplay of close binaries (mass transfer), these systems provide a wealth of data for us to explore.
3. **Planetary Detectives:** Ever wondered if a star has hidden companions? Eclipsing binaries can reveal their presence! By meticulously monitoring the timing of eclipses over long periods, astronomers can detect subtle changes that hint at the gravitational tug of unseen planets or brown dwarfs.
4. **Decoding the Light Show:** The intricate dimming patterns observed during eclipses are like secret codes for astronomers. By analyzing these light curves, we can unlock the geometry of the binary system. This allows us to model fascinating effects like limb darkening (stars appearing dimmer at the edges), gravitational brightening (material bulging due to tidal forces), and reflection effects (light bouncing off one star onto the other).
5. **Unraveling the Mystery of M-dwarfs:** These low-mass stars are like cosmic enigmas. Eclipsing binaries with M-dwarf components helps us understand their poorly understood mass-radius relationship. It turns out these stars might be puffier than stellar models predict!
6. **Mass Transfer Masters:** Semi-detached binaries offer a clear view of the dynamic dance of mass transfer in close binary systems. We can study the flow of stellar material, how it accretes onto the companion star, and even witness the formation of hot spots due to this energetic process.
7. **Overcontact Enigmas:** Overcontact binaries are a puzzle waiting to be solved. Though abundant, they remain poorly understood. By meticulously modeling these systems, astronomers are working to unravel their population frequency and structure, shedding light on these enigmatic cosmic couples.

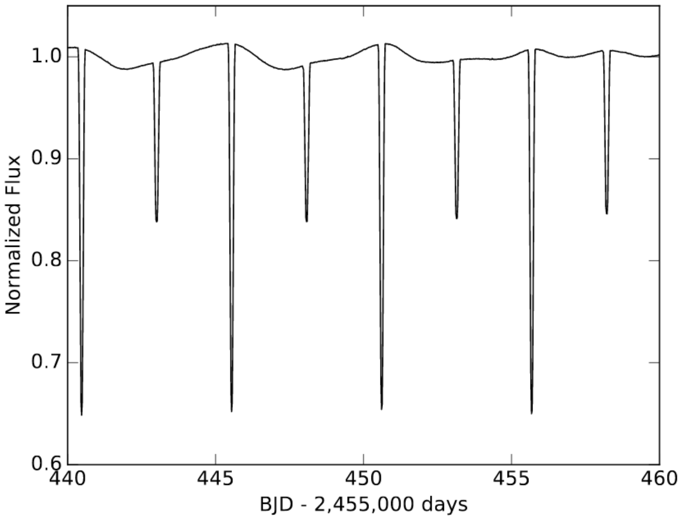

Figure 4.7: Light curve of KIC 8736245 obtained by Kepler Space Telescope

4.3 Observations

To study various properties of the eclipsing binary system we first make the following three fundamental observations:-

- The light curve.
- The spectra of each star are measured at several locations in its orbit.
- The apparent magnitude of the system.

Using these three we then calculate all the required properties of the system.

So, we have four pairs of eclipses in the light curve below. If we zoom in on each of the two eclipses of a particular pair, we see that one is deeper than the other; we call the deeper one the **primary eclipse**, and the shallower one the **secondary eclipse**.

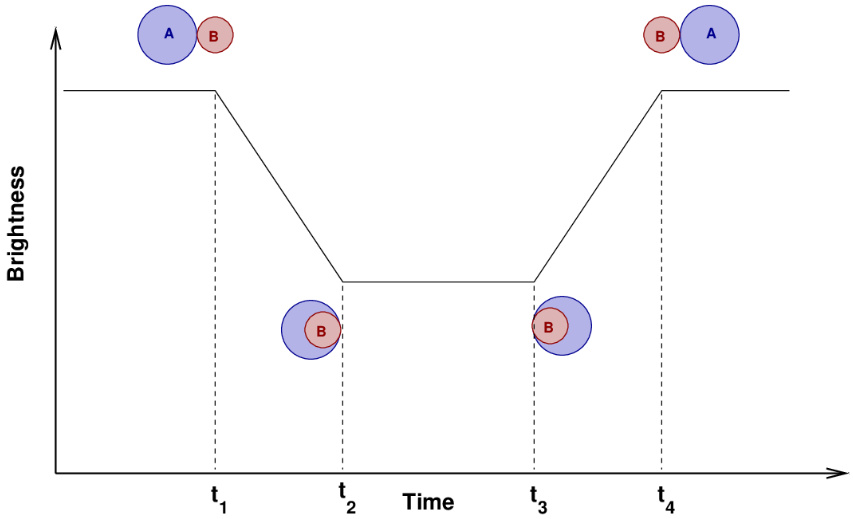

Figure 4.8: Four instances of time in an eclipse

4.4 Estimation of parameters

- **Orbital Period:** The orbital period can be easily calculated from Fig. 4.7 by taking the difference between two successive primary or secondary eclipses.
  We can take the light curve of any particular eclipse, zoom in and make note of the following time instances as shown in the fig. below.

  For this introduction, we'll just assume that this orbit is perfectly edge-on (or the inclination is zero), which simplifies all the calculations.

- **Radial and Orbital velocities:** For finding the radial velocities, we use the spectra of the stars. The Doppler shift of the lines yields the radial velocity of each star. Then, assuming that the stars are orbiting around their centre of mass in circular orbits, we can conclude that the radial velocities of the stars away or towards us are themselves the orbital velocities around the centre of mass. Let's denote them by v_A and v_B.

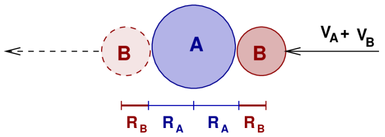

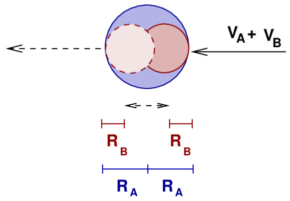

- **Radii:** From these two figures, we can easily get the following equations:

$$2R_A + 2R_B = (v_A + v_B)(t_4 - t_1) \tag{4.1}$$

$$2R_A - 2R_B = (v_A + v_B)(t_3 - t_2) \tag{4.2}$$

  So we have two equations with two unknowns from which the radii can easily be found.
- **Masses:** Now, what about the individual masses? From Kepler's Third Law, we have:

$$P^2 = \frac{4\pi^2}{G(m_1 + m_2)}a^3, \text{ where } \; a = r_A + r_B \tag{4.3}$$

  Here,
  - P = Period of orbit
  - G = Universal Gravitational Constant
  - m_1 and m_2 are the masses of the stars.
  - a = $r_A + r_B$ is the semi-major axis of the orbit.

  From this equation, we can therefore derive $m_1 + m_2$. As the total momentum w.r.t the centre of mass is conserved, we then have:

$$m_A v_A = m_B v_B \tag{4.4}$$

$$\implies \frac{v_A}{v_B} = \frac{m_B}{m_A} \tag{4.5}$$

  Therefore, using the ratio and sum of the masses we can obtain their individual masses.
- **Temperatures:** We now try to make a rough estimation of the temperatures of our stars.

  During one full orbit, each star goes behind the other one, thus forming the primary and secondary eclipses. The temperatures of both the stars may be different, one being hotter than the other. It's easy to follow from here that the primary eclipse (having a deeper dip) is the case of a cooler star eclipsing the hotter one, and the secondary eclipse is quite the opposite. Now let the temperatures of these stars be denoted by T_A and T_B and the radii be R_A and R_B.

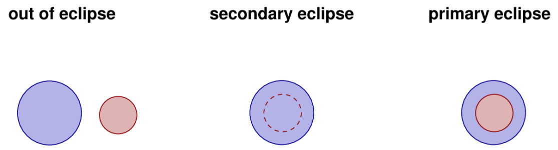

From the above figure, we can find the total brightness at each of these moments (assuming the stars radiate as blackbodies).

$$B_{tot} = 4\pi R_A^2 \sigma T_A^4 + 4\pi R_A^2 \sigma T_A^4 \tag{4.6}$$

$$B_{sec} = 4\pi R_A^2 \sigma T_A^4 \tag{4.7}$$

$$B_{pri} = 4\pi (R_A^2 - R_B^2) \sigma T_A^4 + 4\pi R_A^2 \sigma T_A^4 \tag{4.8}$$

Making some algebraic manipulations, we can obtain the following result:

$$\frac{B_{tot} - B_{pri}}{B_{tot} - B_{sec}} = \left(\frac{T_A}{T_B}\right)^4 \tag{4.9}$$

We know the brightnesses from the light curve, thereby getting the ratio of the temperatures. Let's remember something about dips in the spectra of light curves at different positions in their orbit. Doesn't the ratio signify something?
Well, the dips depend upon the size and temperature of the binary pairs. So, in this case, assuming T_A is greater than T_B, we can conclude that $B_{tot} - B_{pri}$ is lower than $B_{tot} - B_{sec}$. So now we know why there is one dip shallower than the other.

This is a particular case for understanding about the dips in light curve, things will change if our line of sight is inclined at an angle with the plane of the Binaries and calculations will be tidious than before.

But we could just find an estimated ratio of the temperatures. In order to properly calculate the temperatures of the stars, one needs to compute a full spectral model of each star's photosphere, which will depend on the chemical composition, mass, age, and other factors. It's a job quite difficult for us, but astronomers who specialize in the analysis of eclipsing binaries have developed tools to do all this work.

- **Luminosity:** Now let's assume we have the individual temperatures of these stars after taking into account the above factors. Then how to get their luminosities? If we continue to assume that the stars emit like blackbodies, then the total energy emitted by the pair can simply be given by:

$$L = 4\pi R_A^2 \sigma T_A^4 + 4\pi R_A^2 \sigma T_A^4 \tag{4.10}$$

- **Distance from us:** Now that we have the luminosity and if we can add just one more piece of information, i.e. its the apparent magnitude, we can get the distance

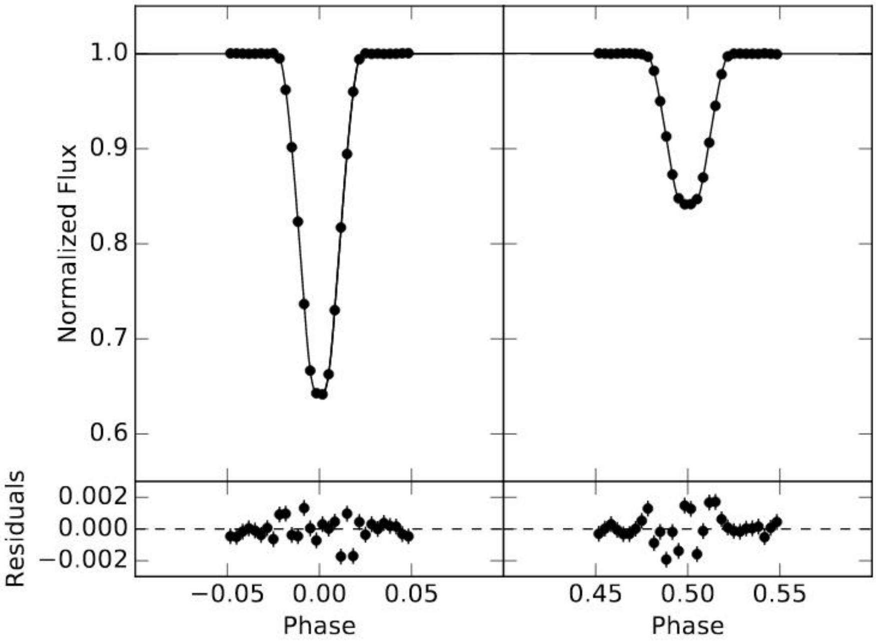

Figure 4.9: Primary And Secondary Eclipse Light Curve

to the system! So what exactly is the Apparent magnitude?

Apparent magnitude is a logarithmic number that measures how bright the object appears from a distance. The absolute magnitude of a celestial object is defined as the magnitude it would have if observed from a standard distance of 10 parsecs.

The following is the relation between them:-

$$m - M = -2.5 \log_{10} \left(\frac{F_m}{F_M} \right) \tag{4.11}$$

Here,

- m is the apparent magnitude
- M is the absolute magnitude
- F_m is the flux observed at a particular distance
- F_M is the flux observed at the fixed distance $d_o = 10\, parsecs$

Now putting the relation between Flux and Luminosity, which is:

$$F = \frac{L}{4\pi d^2} \tag{4.12}$$

in Eq. 4.11, we get:

$$m - M = 5 \log_{10} \left(\frac{d}{d_o} \right) \tag{4.13}$$

where,

- d is distance to the star
- $d_o = 10\, parsecs$

Now the absolute magnitude of our star can be obtained from the following equation:

$$M = 4.83 - 2.5 \log_{10} \left(\frac{L}{L_o} \right) \tag{4.14}$$

where,

- M is the absolute magnitude of our star.
- 4.83 is the absolute magnitude of the Sun.
- L and L_o are the luminosities of the star and the Sun respectively.

Now, we can use Eq. 4.14 to find the absolute magnitude of our system given their luminosity (Eq. 4.10). Using that, the apparent magnitude of our system and Eq.4.13, we can finally obtain the distance to the binary system.

II

Part Two

5 Introduction to `PHOEBE` 53
5.1 Why use `PHEOBE` ?
5.2 Basics of Bundle
5.3 Constraints
5.4 Datasets
5.5 Compute
5.6 Times and Phases

6 Forward Model 63
6.1 What's Forward Modeling?
6.2 Applications of Forward Modeling in Eclipsing Binaries
6.3 Key Steps for Forward Modeling with `PHOEBE`
6.4 DI Herculis: Misaligned binary

7 Inverse problem 73
7.1 Estimators
7.2 Merit Function
7.3 Optimizers
7.4 Samplers
7.5 Posteriors & Uncertainties

Bibliography 85

Index 89

5. Introduction to `PHOEBE`

Physics Of Eclipsing BinariEs (`PHOEBE`) is a powerful and versatile Python package designed specifically for the analysis and modeling of eclipsing binary stars. Leveraging advanced algorithms and robust data processing capabilities, `PHOEBE` provides astronomers and astrophysicists with a comprehensive toolkit for simulating and interpreting the complex interactions between binary star systems. It helps in reproducing and fitting light curves, radial velocity curves, and spectral line profiles of eclipsing binaries.

5.1 Why use `PHEOBE` ?

- **Superior Accuracy and Robustness:** Compared to other binary star analysis models such as `JKTEBOP` and `ELLC`, `PHOEBE` offers significantly higher accuracy and robustness.
- **Advanced Physical Effects:** One of `PHOEBE`'s most distinguishing features is its ability to incorporate a wide array of advanced physical effects that other models cannot handle effectively. These include:
  - **Spots:** The ability to model star spots, which can affect the light curves of binary systems.
  - **Beaming:** The model accounts for relativistic beaming, where the light from a star is concentrated in the direction of its motion.
  - **Heartbeat Binaries:** `PHOEBE` can accurately model heartbeat binaries, systems where the stars have highly eccentric orbits leading to brief but significant variations in brightness.
  - **Rossiter-McLaughlin (RM) Effect:** The model includes the RM effect, a phenomenon observed during transits that provides information on the spin-orbit alignment of the stars.
  - **Tidal Distortion and Reflection:** It also models the effects of tidal forces and mutual reflection between the stars, further the accuracy of its predictions.
- **Comprehensive Forward and Inverse Modeling:** It provides a complete

one-stop solution for performing both forward and inverse modeling.
- **Extensive Documentation:** Despite its complexity, PHOEBE is designed with the user in mind, offering extensive documentation. This makes it accessible to both seasoned researchers and those new to the field, allowing for easy adoption and integration into various research workflows.

5.2 Basics of Bundle

In PHOEBE, a "bundle" serves as a comprehensive container for all parameters used within the package. Managing and organizing these parameters is essential, given the complexity and the sheer number of parameters involved in modeling binary star systems. Bundles facilitate this organization by grouping related parameters and providing a structure for accessing and modifying them efficiently.

A bundle in PHOEBE is a collection of parameters along with callable methods. Each parameter within the bundle is a Python object, and PHOEBE comprises over 140 individual parameters. These parameters are uniquely identified by a set of tags. For instance, there are six different contexts in which a parameter may be used: *system, component, constraint, figure, setting*, and *compute*. The *compute* tag, for example, determines how a forward model is calculated. These tags allow for filtering and selecting parameters based on specific needs.

Each floating-point parameter in PHOEBE is also associated with a unit, ensuring consistency in calculations and interpretations across different scales and contexts.

5.3 Constraints

The parameters defined within a Bundle in PHOEBE are not entirely independent; many are interconnected through relationships known as constraint equations. These constraints enforce specific dependencies between parameters, ensuring consistency across the model. For example, the inclination of the primary star is constrained to match the inclination of the binary orbit if the pitch is set to zero. As a result, any modification to the orbital inclination will automatically update the inclinations of both the primary and secondary stars to maintain this relationship.

In binary star systems, a significant number of parameters are constrained by such relationships. A notable example is the interdependence of four key parameters: the semi-major axis (sma), the orbital period, the mass ratio (q), and the total mass. These parameters are linked by Kepler's Third Law, which dictates that setting any three of these parameters allows PHOEBE to automatically compute the fourth. Furthermore, PHOEBE provides the flexibility to reparameterize or alter the constraint relation, enabling the calculation of any one parameter based on the values of the other three.

This system of constraints is essential for maintaining the physical realism and consistency of the model, allowing for dynamic updates and ensuring that all parameters are in harmony with the underlying astrophysical principles.

5.4 Datasets

In PHOEBE, data management is facilitated through dedicated datasets, which can either consist of actual observational data or parameterize the forward-model observables that PHOEBE can synthesize. The following types of datasets are supported:

- **lc** (light curves)
- **rv** (radial velocity curves)
- **lp** (line profiles)
- **orb** (orbits)
- **mesh** (meshes)

Each dataset type serves a distinct purpose and can be added to a bundle in specific ways, as described below:

5.4.1 Light Curves (lc)

A light curve (lc) graphically represents the light intensity of a celestial object over time. To include an LC dataset in the bundle, use the following method:

```
b.add_dataset('lc', times=phoebe.linspace(0, 1, 51), dataset='lc01')
```

By filtering based on the dataset, you can retrieve the associated parameters:

```
b.filter(dataset='lc01').contexts
```

This step confirms that the `lc01` dataset has been successfully integrated, including all necessary parameters.

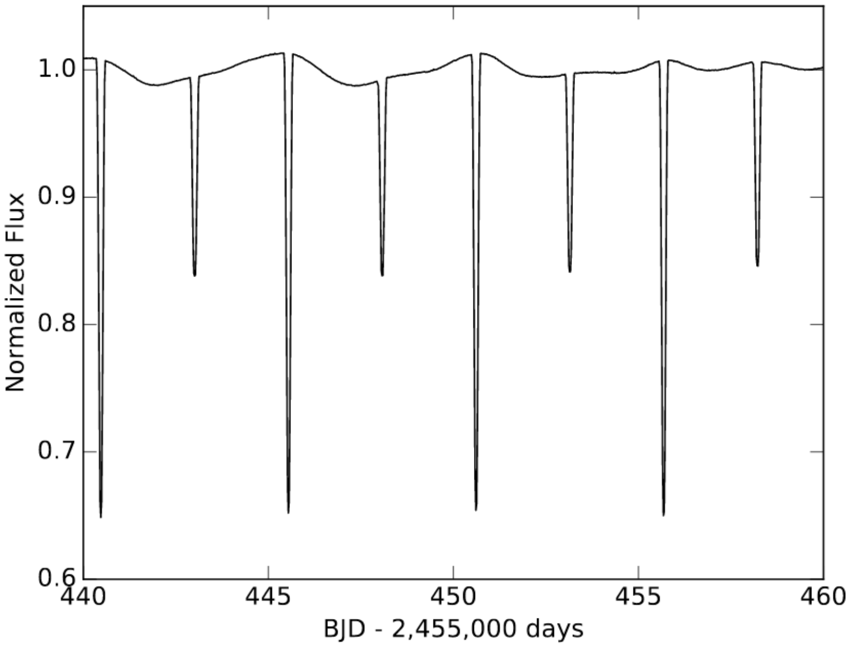

Figure 5.1: Plot of synthetically generated light curve data for the 'lc' dataset.

5.4.2 Radial Velocities (rv)

Radial velocity (rv) measures the velocity of a star or object along the observer's line of sight. To add an RV dataset, use:

```
b.add_dataset('rv', times=phoebe.linspace(0, 1, 11), dataset='rv01')
```

To view all relevant parameters for the `rv01` dataset, filter as follows:

```
b.filter(dataset='rv01', context='dataset').qualifiers
```

This step indicates that the `rv01` dataset has been added, including components for both the primary and secondary objects.

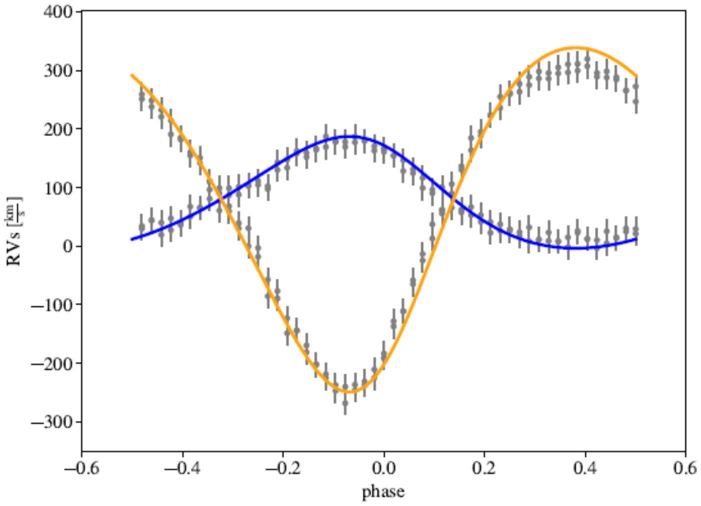

Figure 5.2: Plot of synthetically generated radial velocity data for the 'rv' dataset.

5.4.3 Line Profiles (lp)

Line profiles represent the variation of light intensity with wavelength, typically associated with spectral lines. Once added, the times in this dataset cannot be modified, although wavelengths can be adjusted. To add this dataset, use:

```
b.add_dataset('lp', times=phoebe.linspace(0, 1, 11), wavelengths=
                phoebe.linspace(549, 551, 101), dataset='lp01')
```

Inspect the parameters for the `lp01` dataset in the 'dataset' context:

```
b.filter(dataset='lp01', context='dataset').qualifiers
```

The `lp01` dataset is now successfully included, complete with all necessary components.

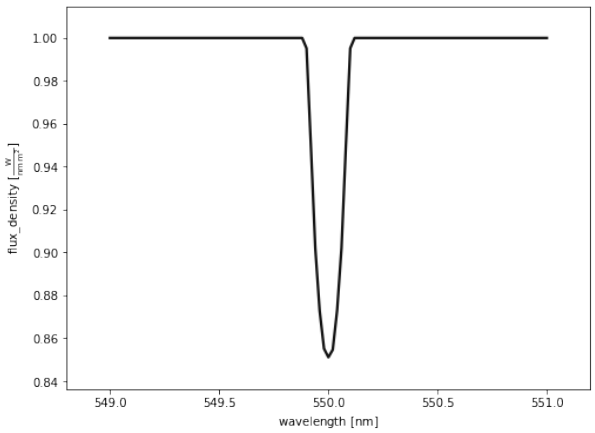

Figure 5.3: Plot of synthetically generated light profile data for the ’lp’ dataset.

5.4.4 Orbits (orb)

The orbit (orb) dataset simulates the orbital motion of stars within a system at specified times, which is particularly useful for visualization. To add an ORB dataset, use:

```python
b.add_dataset('orb', compute_times=phoebe.linspace(0, 1, 101),
                dataset='orb01')
```

Orbits are parameterized by compute times or phases, and any provided times will be adopted as compute times. Filter the qualifiers for the `orb01` dataset as follows:

```python
b.filter(dataset='orb01', context='dataset').qualifiers
```

```python
b.filter(dataset='orb01', context='compute').qualifiers
```

This confirms that the `orb01` dataset has been correctly added, including all orbit-related components.

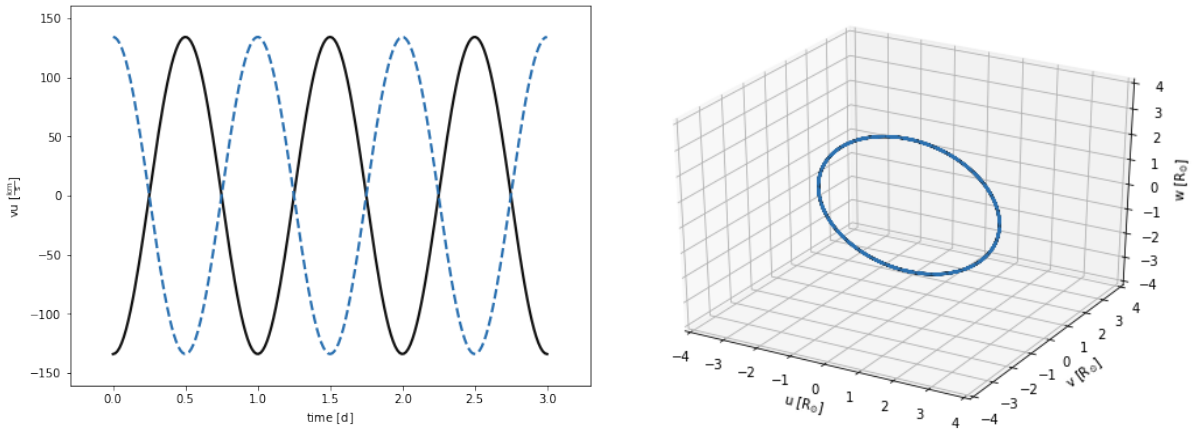

(a) Orbit in 2D

(b) Orbit in 3D

Figure 5.4: Combined figure of 2D and 3D orbits obtained from PHOEBE.

5.4.5 Meshes

The mesh dataset is used to visualize the geometry of a system over time. Unlike observational datasets, meshes are essential for visualization rather than direct data analysis. Meshes are parameterized by compute times, derived from any times provided during dataset creation:

```
b.add_dataset('mesh', compute_times=[0, 0.5, 1], dataset='mesh01')
```

Review the parameters within the ’dataset’ and ’compute’ contexts for the `mesh01` dataset:

```
b.filter(dataset='mesh01', context='dataset').qualifiers
```

With this, the `mesh01` dataset is successfully added, completing the dataset integration process.

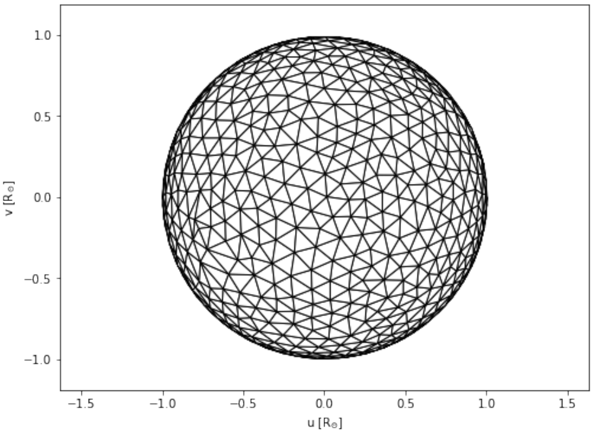

Figure 5.5: Plot of synthetically generated Triangular Meshing data for the ’mesh’ dataset.

5.5 Compute

To initiate the modeling process in `PHOEBE`, we start by adding simple datasets:

```
b.add_dataset('lc', compute_times=phoebe.linspace(0,1,51),
                dataset='lc01')
b.add_dataset('rv', compute_times=phoebe.linspace(0,1,21),
                dataset='rv01')
```

These commands incorporate light curve (lc) and radial velocity (rv) datasets with specified time grids. To compute the forward model using default settings, execute the following command:

```
b.run_compute()
```

This command generates synthetic versions of the datasets, tagged with `context=’model’`. To inspect these models, use the following commands:

```
b.filter(context='model').datasets
b.filter(context='model', dataset='lc01')
```

By default, models are tagged as 'latest' and will be overwritten in subsequent computations unless a unique model tag is specified. To explicitly tag a model, use:

```
b.run_compute(model='mymodel')
```

For light curves, the synthetic model includes times and fluxes. Access these parameters with:

```
b.get_parameter(context='model', dataset='lc01', qualifier='times')
b.get_parameter(context='model', dataset='lc01', qualifier='fluxes')
```

For radial velocities, the synthetic model provides times and radial velocities for each star. To retrieve parameters for a specific component, use:

```
b.filter(context='model', dataset='rv01').qualifiers
b.get_parameter(context='model', dataset='rv01',
                component='primary', qualifier='rvs')
b.get_parameter(context='model', dataset='rv01',
                component='secondary', qualifier='rvs')
```

5.5.1 Custom Compute Options

Compute options, which control the methods and effects of computations, are defined with `context='compute'`. To list the default options, use:

```
print(b.filter(context='compute').qualifiers)
```

To create a new set of compute options, such as for quick computations, use:

```
b.add_compute(compute='preview')
```

To view and modify specific compute parameters:

```
b.filter(context='compute', qualifier='ltte')
b.set_value(qualifier='ltte', context='compute', compute='preview',
            value=False)
```

For parameters with multiple components, set values for all components simultaneously:

```
b.set_value_all(qualifier='rv_grav', context='compute',
                compute='preview', value=False)
```

Parameters such as `irrad_method` can be modified similarly:

```
b.get_parameter(context='compute', compute='preview',
                qualifier='irrad_method').choices
b.set_value(qualifier='irrad_method', context='compute',
```

```python
                compute='preview', value='none')
b.set_value_all(qualifier='ntriangles', context='compute',
                compute='preview', value=800)
```

To re-run computations with custom options, specify the compute option:

```python
b.run_compute(compute='preview')
```

5.5.2 Temporarily Overriding Options

Compute options can be temporarily overridden for a single run:

```python
b.run_compute(compute='preview', irrad_method='horvat')
b.run_compute(compute='preview', times=[0, 0.5, 1])
```

To check the times used in datasets and models, use:

```python
print("dataset times: ", b.get_value('compute_times', dataset='lc01',
        context='dataset'))
print("model times: ", b.get_value('times', dataset='lc01',
        context='model'))
```

5.5.3 Alternate Backends

Compute options also support running different backends. To use an alternate backend, such as PHOEBE 1.0, add it with:

```python
b.add_compute('legacy', compute='legacycompute')
```

To inspect parameters for the alternate backend, use:

```python
print(b.filter(compute='legacycompute'))
```

5.6 Times and Phases

PHOEBE operates in time-space, which facilitates the accurate parametrization of time-dependent quantities. However, challenges arise when data is provided in phase space or when a phased light curve is required. To address these challenges, PHOEBE offers methods to convert between time and phase spaces.

Converting between time and phase relies on the following parameters:

- **period** (the orbital period of the binary at reference time t_0)
- **dpdt** (the rate of change of the orbital period over time)
- **t0** (the reference time-point)

The reference time-point t_0 can be defined using several conventions, as specified in the bundle:

- `t0_supconj`: time of superior conjunction
- `t0_perpass`: time of periastron passage
- `t0_ref`: time of the reference point with respect to apsidal motion

By default, `t0_supconj` is a free parameter, whereas `t0_perpass` and `t0_ref` are constrained by other parameters. To retrieve these parameters, use the following commands:

```
b.get_parameter(qualifier='t0_supconj', context='component')
b.get_parameter(qualifier='t0_perpass', context='component')
b.get_parameter(qualifier='t0_ref', context='component')
```

For demonstration purposes, to change the orbital period such that the times and phases are affected, use:

```
b.set_value(qualifier='period', component='binary', value=2.5)
```

The `get_ephemeris()` method provides the current ephemeris of the system for any predefined t_0 or custom time:

```
b.get_ephemeris(t0='t0_supconj')
b.get_ephemeris(t0='t0_perpass')
b.get_ephemeris(t0=5)
```

To convert times to phases, utilize the `to_phase()` method:

```
b.to_phase([0, 0.1], t0='t0_supconj')
b.to_phase([0, 0.1], t0='t0_perpass')
```

To convert phases back to times (specifically, the first instance of the phase after the provided t_0), use `to_time()`:

```
b.to_time(0.5, t0='t0_supconj')
b.to_time(0.5, t0=2455000)
```

5.6.1 Compute Phases

Datasets in PHOEBE can include a `compute_phases` parameter, which enables phase-space computations. To compute a model in phase-space, use:

```
b.add_dataset('lc', compute_phases=phoebe.linspace(0, 1, 101),
             dataset='lc01')
```

To view compute times and phases, execute:

```
print(b.filter(qualifier=['compute_times', 'compute_phases'],
             context='dataset'))
```

If the orbital period is modified, use the following commands to observe changes:

```
b.set_value('period', component='binary', value=3.14)
print(b.filter(qualifier=['compute_times', 'compute_phases'],
             context='dataset'))
```

Important: Do not use `compute_phases` to convert between times and phases if your data is already in phases. Instead, convert phases to times using `to_time()` with the original ephemeris information:

```
phases = phoebe.linspace(0, 1, 101)
times = b.to_time(phases, t0=2459752.18750)
b.add_dataset('lc', times=times, fluxes=phoebe.linspace(1, 1, 101))
```

An extra caution should be exercised using the "`compute_phases`" command when the data is in phases. Therefore, the user needs to first convert the phases to times...

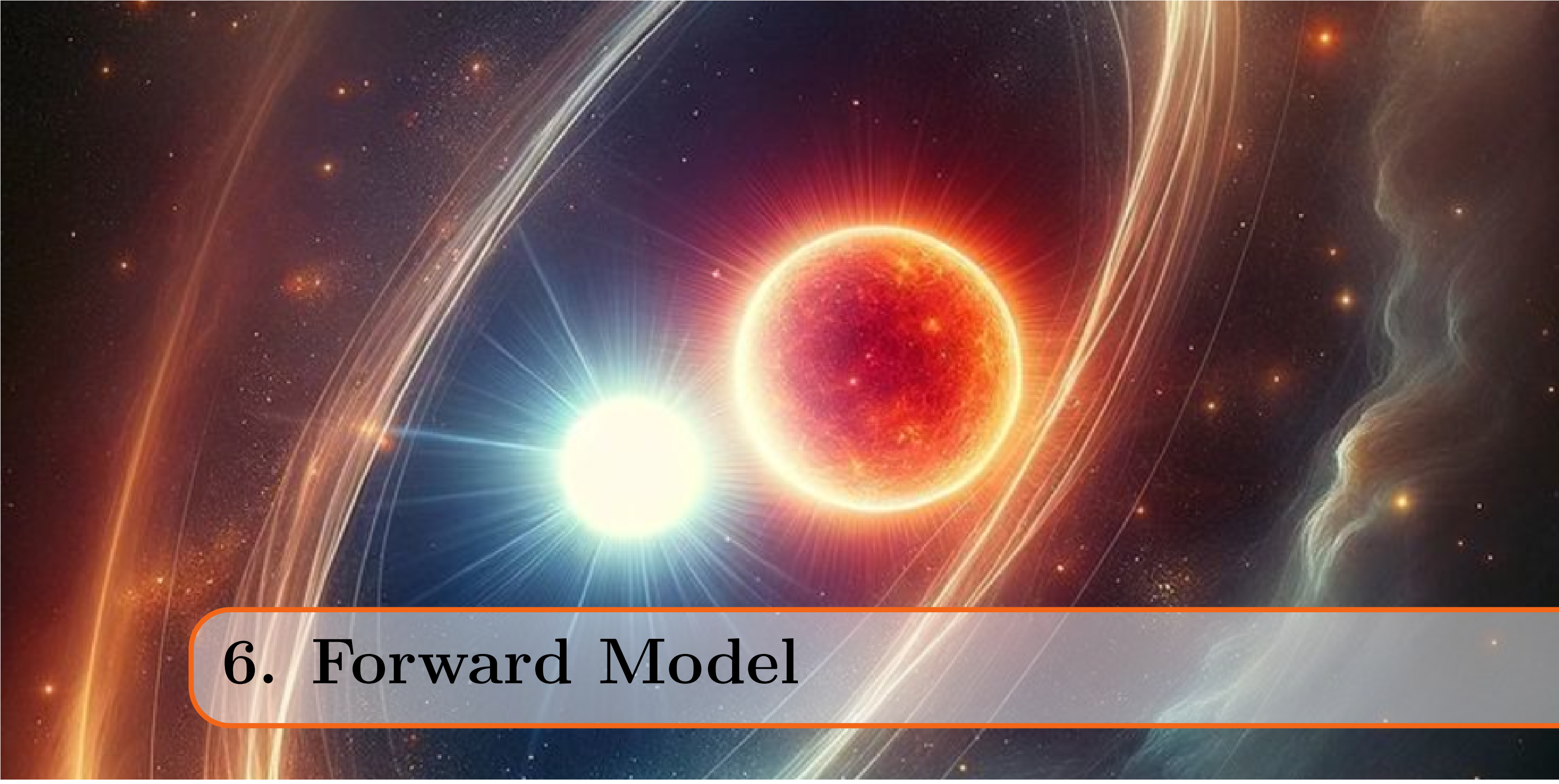

6. Forward Model

6.1 What's Forward Modeling?

Forward modeling is a computational process where a mathematical model is used to predict the outcome of a system based on a set of input parameters. It's essentially a simulation of a real-world process. The model encapsulates our understanding of the system's underlying physics or other relevant principles.

For example, it is a powerful tool for studying eclipsing binary stars. In essence, it involves creating a theoretical model of the binary system based on assumed or observed physical parameters of a system, such as the masses, radii, temperatures, and orbital elements of each star, and then simulating the physical processes and interactions within an eclipsing binary star system to predict expected light curve and other observations that would result from such a system.

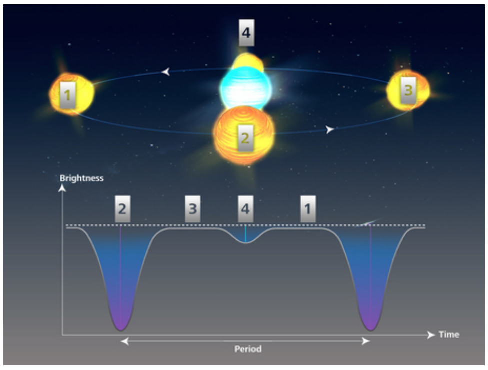

Figure 6.1: Eclicing binary Model

Why is Forward Modeling used?

Forward modeling is essential for understanding and analyzing causal relationships, including identifying key factors, and is fundamental to effective research and modeling.

Researchers can construct robust models capable of simulating various scenarios by testing and refining theoretical frameworks. This approach enables the extraction of valuable insights from data patterns, uncovering latent properties and informing predictive capabilities. Ultimately, these methodologies contribute to the assessment of potential risks and the forecasting of future events.

Other Examples In Astrophysics where Forward Modeling is used:

- **Exoplanet Detection and Characterization:** Simulating the transit depth and shape of an exoplanet passing in front of its host star based on assumed planetary properties.

- **Stellar Astrophysics:** Creating models of stellar interiors and atmospheres to predict observable properties like luminosity, temperature, and spectral energy distribution and to study stellar evolution.

- **Galaxy Formation and Evolution:** Simulating the formation and evolution of galaxies based on cosmological parameters, initial conditions, and physical processes like star formation, galaxy mergers, and feedback mechanisms.

- **Cosmic Microwave Background (CMB):** Generating simulated CMB maps based on cosmological models, including parameters like dark matter density, baryon density, and the amplitude of primordial fluctuations.

6.2 Applications of Forward Modeling in Eclipsing Binaries

- **Model Validation**: By comparing the forward-modelled light curve with the observed one, we can assess the accuracy of our physical model.

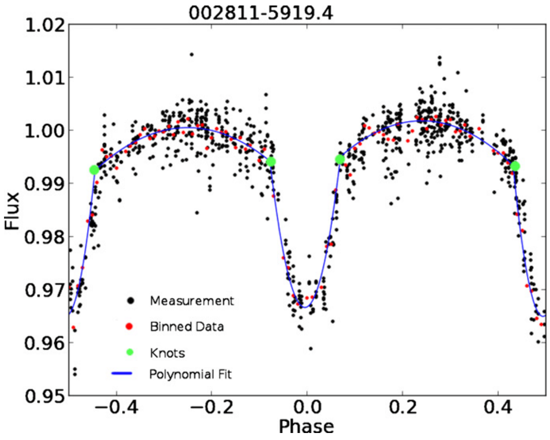

Figure 6.2: Model validation using light curve

- **Prediction:**Once a reliable model is established, it can predict the system's behavior under different conditions or at different times.

- **Understanding Physical Processes:** By experimenting with different model parameters, we can gain insights into the physical processes, such as mass transfer at play in the binary system.

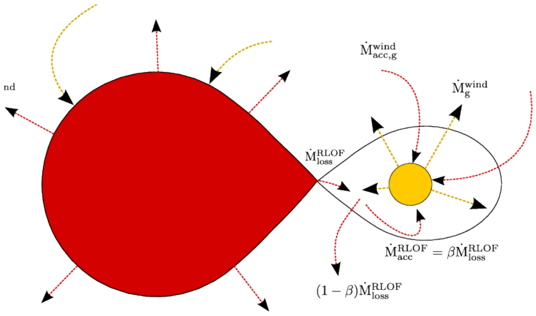
nd
$\dot{M}^{\rm wind}_{\rm acc,g}$
$\dot{M}^{\rm wind}_{\rm g}$
$\dot{M}^{\rm RLOF}_{\rm loss}$
$\dot{M}^{\rm RLOF}_{\rm acc} = \beta\dot{M}^{\rm RLOF}_{\rm loss}$
$(1-\beta)\dot{M}^{\rm RLOF}_{\rm loss}$

Figure 6.3: Mass Transfer

- **Studying Stellar Evolution:** Forward modeling can help understand how stars evolve with theoretical models of stellar structure.

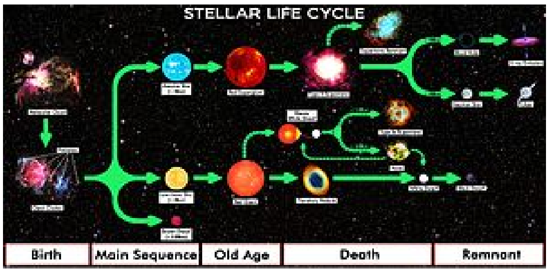
STELLAR LIFE CYCLE
Birth
Main Sequence
Old Age
Death
Remnant

Figure 6.4: Stellar evolution

- **Discover new phenomena:** Sometimes, unexpected features in the observed light curve can hint at new physical processes, which can be explored through forward modeling.

6.3 Key Steps for Forward Modeling with `PHOEBE`

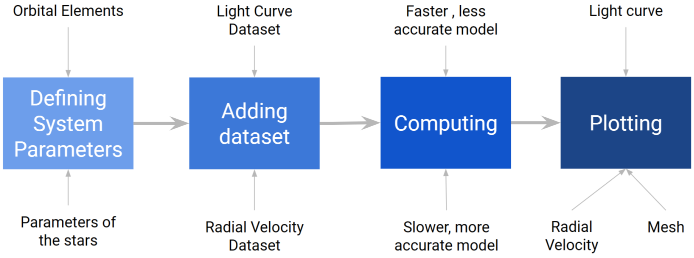
Orbital Elements
Defining System Parameters
Parameters of the stars
Light Curve Dataset
Adding dataset
Radial Velocity Dataset
Faster , less accurate model
Computing
Slower, more accurate model
Light curve
Plotting
Radial Velocity
Mesh

Figure 6.5: Key Steps for Forward Modeling with `PHOEBE`

We first import `PHOEBE` and initialize a logger and a new bundle.
Example snippet :

```python
import phoebe
import numpy as np

logger = phoebe.logger('error')

b = phoebe.default_binary()
```

6.3.1 Defining System Parameters:

while creating the forward model, we set the parameters of the eclipsing binary system. The following properties are used to define a system.

Stellar properties:
- Masses (m),
- Radii (R),
- Temperatures(T),
- Luminosities(L),
- Gravities,
- Limb darkening,
- Coefficients,
- etc., for both the components stars.

Orbital elements:
- Period (T),
- Semimajor axis(a),
- Eccentricity(e),
- inclination(i),
- the longitude of the ascending node(Ω),
- the argument of periapsis(ω),
- and time of periapsis passage.

Geometric parameters:
- Spot parameters (if present)'
- tidal distortion,
- etc., for both the component stars.

While setting the values of these parameters in default parameterization, some of them are constrained by other parameters, and therefore, we can set values for these parameters by setting the value of the constraining parameters or by re-parameterization (Constraints were extensively discussed in section 5.3).
setting the values of some of the parameters in this example snippet: here, the values that have been taken are from Bell u.a. (1987).

```python
b.set_value('q', 0.360) #mass ratio
b.set_value('sma@binary', 21.585261164816995) #Semimajor axis
b.set_value('incl@binary', 61.30000) #incilnation
b.set_value('ecc@binary', 0.) #eccentricity
b.set_value('period@binary', 1.621887) #period

#Bolometric gravity brightening parameter
b.set_value('gravb_bol@primary', 1.)
```

```python
b.set_value('gravb_bol@secondary', 1.)

#Synchronicity parameter
b.set_value('syncpar@primary', 1.0)
b.set_value('syncpar@secondary', 1.0)

#Yaw of the stellar rotation axis
b.set_value('yaw@primary',2.886187)
b.set_value('yaw@secondary',2.683761)

#Mean effective temperature
b.set_value('teff@primary', 35600.)
b.set_value('teff@secondary', 27470.)

#Equivalent radius
b.set_value('requiv@primary', 8.8)
b.set_value('requiv@secondary',5.9)
```

6.3.2 Adding dataset:

Now, after setting the parameters for the binary system, we synthesize the dataset using `PHOEBE` for the example light curve and radial velocity data set (datasets were extensively discussed in section 5.4).
adding dataset for lightcurve, radial velocity, and mesh in this example snippet:

```python
times = b.to_time(np.linspace(-0.05, 1.05, 200))
b.add_dataset('lc', times=times, dataset='lc01') #Lightcurve
b.add_dataset('rv', times=times, dataset='rv01') #Radial velocity
b.add_dataset('mesh',compute_times=np.linspace(0,1,201),dataset='mesh01')
```

6.3.3 Computing:

Now, using compute `PHOEBE`, we will calculate the theoretical curves for the dataset chosen in the previous step based on the input parameters. Computing can be done with several methods, from less accurate models to very accurate models at the cost of computing time (Computing was extensively discussed in section 5.5).
let's take a look at an example snippet of computing where we have run the default compute command:

```python
b.run_compute()
```

6.3.4 Ploting:

Now, we plot the curves of the dataset and analyze and visualize the system that has been modeled. We analyze the generated light and radial velocity curves and compare them to observed data (if available) to assess the model's accuracy and use the `PHOEBE` tools to visualize the system geometry and other parameters. Additionally, we can compare different computing options. we plot the graphs like the following example snippet:

```
    afig, mplfig = b.plot(dataset='lc01',show=True)
```

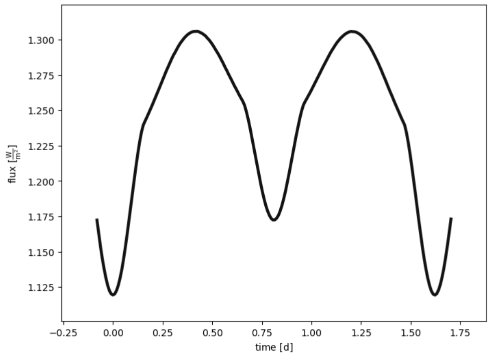

Figure 6.6: Output of the Light curve graph

```
afig, mplfig = b.plot(dataset='rv01',show=True), show=True)
```

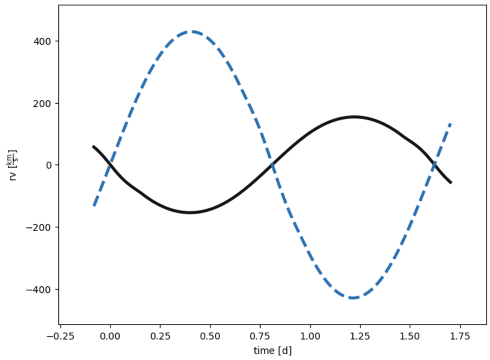

Figure 6.7: Output of the Radial velocity graph

```
afig, mplfig = b.plot(dataset='mesh01',time=0.4, show=True)
```

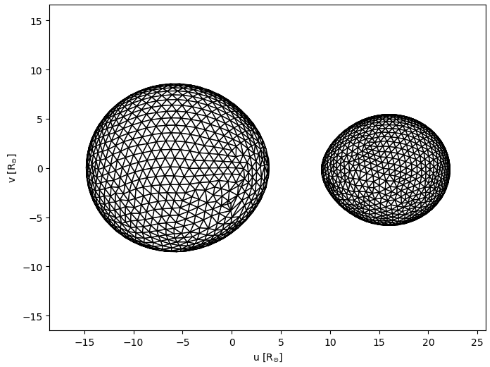
15
10
5
0
−5
−10
−15
v [R$_\odot$]
−15
−10
−5
0
5
10
15
20
25
u [R$_\odot$]

Figure 6.8: Mesh of the Binary system

6.4 DI Herculis: Misaligned binary

Now, let's take a look at the code for DI Herculis, a misaligned system. First, we import `PHOEBE` and initialize a logger and a new bundle.

```
import phoebe
from phoebe import u # units
import numpy as np
import matplotlib.pyplot as plt

logger = phoebe.logger('error')

b = phoebe.default_binary()
```

Next, we define the System Parameters. We'll adopt and set parameters from the following sources:

- Albrecht u.a. (2009)
- Claret u.a. (2010)
- DI Herculis. (2023, May 11). In Wikipedia https://en.wikipedia.org/wiki/DI_Herculis

```
Nt = 2000

b.set_value('t0_supconj@orbit', 2442233.3481)
b.set_value('vgamma@system', 9.1) # [km/s] (Albrecht et al. 2009)
b.set_value('ntriangles@primary', Nt)
b.set_value('ntriangles@secondary', Nt)

mass1 = 5.1 # [M_sun] (Albrecht et al. 2009)
mass2 = 4.4 # [M_sun] (Albrecht et al. 2009)

P = 10.550164             # [d] (Albrecht et al. 2009)
mu_sun = 1.32712440018e20 # = G M_sun [m3 s^-2],
R_sun = 695700000         # [m] Wiki Sun

sma = (mu_sun*(mass1 + mass2)*(P*86400/(2*np.pi))**2)**(1./3)/R_sun

incl = 89.3   # deg (Albrecht et al. 2009)
vp_sini = 109 # [km/s] (Albrecht et al. 2009)
vs_sini = 117 # [km/s] (Albrecht et al. 2009)

Rp = 2.68 # [R_sun] (Albrecht et al. 2009)
Rs = 2.48 # [R_sun] (Albrecht et al. 2009)

sini = np.sin(np.pi*incl/180)

vp = vp_sini*86400/sini # [km/s]
vs = vs_sini*86400/sini # [km/s]

```

```
    Pp = 2*np.pi*Rp*R_sun/1000/vp
    Ps = 2*np.pi*Rs*R_sun/1000/vs

    Fp = P/Pp
    Fs = P/Ps

    b.set_value('q', 0.815)
    b.set_value('incl@binary', incl) # (Albrecht et al. 2009)
    b.set_value('sma@binary', sma)   # calculated
    b.set_value('ecc@binary', 0.489) # (Albrecht et al. 2009)

    b.set_value('per0@binary', 330.2) # (Albrecht et al. 2009)
    b.set_value('period@binary', P)   # calculated

    b.set_value('syncpar@primary', Fp)   # calculated
    b.set_value('syncpar@secondary', Fs) # calculated

    b.set_value('requiv@primary', Rp)   # requiv (Albrecht et al. 2009)
    b.set_value('requiv@secondary', Rs) # requiv (Albrecht et al. 2009)

    b.set_value('teff@primary', 17300)    # Wiki DI_Herculis
    b.set_value('teff@secondary', 15400)  # Wiki DI_Herculis

    b.set_value('gravb_bol@primary', 1.)
    b.set_value('gravb_bol@secondary', 1.)


    # beta = 72 deg (Albrecht et al. 2009)
    dOmega_p = 72
    di_p = 62  - incl
    b.set_value('pitch@primary', di_p)   # di
    b.set_value('yaw@primary', dOmega_p) # dOmega

    # beta = - 84 deg (Albrecht et al. 2009)
    dOmega_s = -84
    di_s = 100 - incl
        b.set_value('pitch@secondary', di_s) # di
    b.set_value('yaw@secondary', dOmega_s)   # dOmega

    b.set_value_all('atm','extern_planckint')
    b.set_value_all('irrad_method', 'none')
```

Now let's add an LC and RV dataset sampled at 200 points in phase

```
    n = 200
times = b.to_time(np.linspace(-0.05, 1.05, n))

    b.add_dataset('lc', times=times, dataset='lc01', ld_mode='manual', ld_func='logar
    b.add_dataset('rv', times=times, dataset='rv01', ld_mode='manual', ld_func='logar
    b.set_value('columns', value=['teffs', 'loggs', '*intensities*'])
```

Computing

```
    b.run_compute(ltte=False)
```

Plotting

```
    afig, mplfig = b.plot(kind='lc', show=True)
```

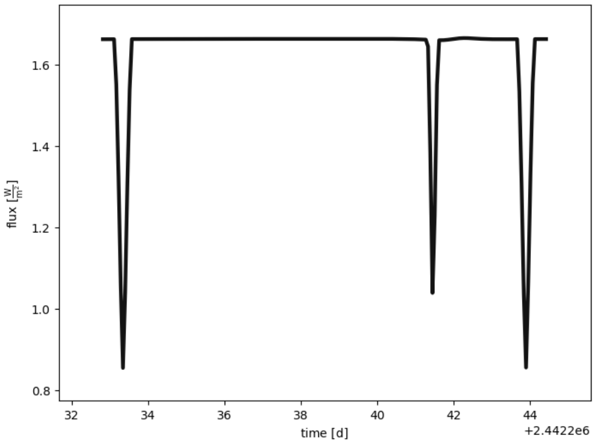

Figure 6.9: Lighr curve of DI-Herculis

```
    afig, mplfig = b.plot(kind='rv', show=True)
```

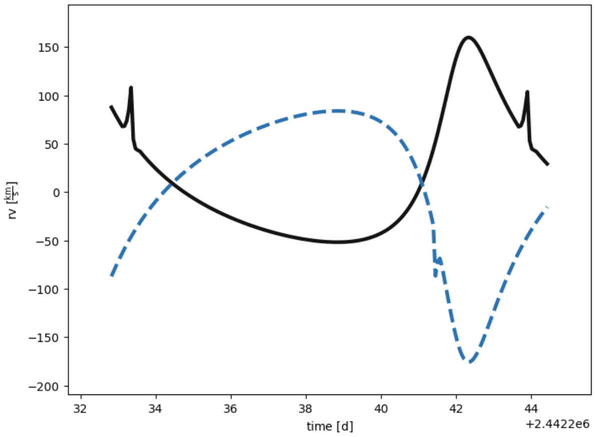

Figure 6.10: Radial velocity curve of DI-Herculis

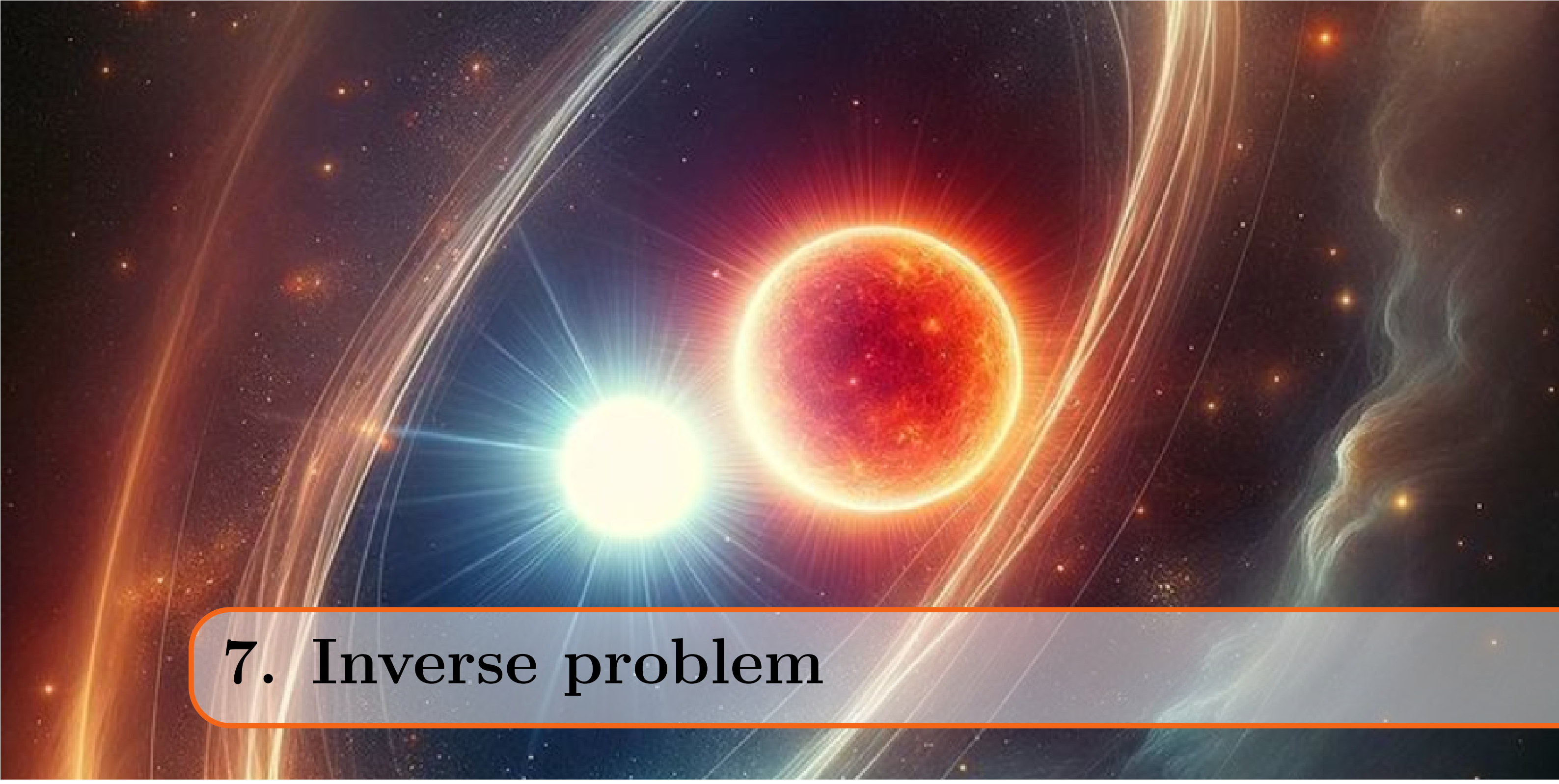

7. Inverse problem

As discussed briefly in Chapter 5, inverse problems start with the observed data in hand. In the case of forward models, we input the period, mass ratio, eccentricity, argument of periastron, radii, temperatures, and other parameters of the eclipsing binary system along with some model defaults like atmospheres and options to compute the forward model. What we get as outputs for the forward model are the observables of the system, like LCs in the requested passband, RVs, or spectral line profiles. The inverse problem is all about finding the correct parameters that would correspond to the observable in hand. However, this problem is more difficult because the observations we make are inherently noisy, which may or may not be stationary. In this chapter, we will see how we can extract the parameters of the system and how we can quantify our lack of certainty in the extracted values of the parameters.

The general framework for utilizing multiple algorithms in `PHOEBE`, informally referred to as the 'phoetting recipe,' involves a systematic approach to parameter estimation and refinement. This recipe begins with **Estimators** (Section 7.1), which propose initial values for various parameters based on observations alone, without the need to compute forward models. These initial estimates are then refined using **Optimizers** (Section 7.3), which run optimization algorithms to improve the parameters by seeking local or global solutions. Finally, **Samplers** (Section 7.4) are employed not to find the global solution but to sample the local parameter space and provide robust posteriors.

7.1 Estimators

It is often useful to estimate the values of parameters from the datasets as input alone without having to compute full forward models. `PHOEBE` includes wrappers around several algorithms (Conroy u.a., 2020) that directly act on the observations themselves to quickly provide initial solutions without significant user supervision.

7.1.1 Periodograms

PHOEBE contains wrappers around two common periodograms - Box Least Squares (BLS), which is well-suited for boxy eclipses of detached stars, and Lomb Scargle (LS), which is more appropriate for stars with strong ellipsoidal variations. hese methods are implemented using `astropy.timeseries` (The Astropy Collaboration u.a., 2013). It is important to note that the radial velocity periodogram only supports the LS algorithm. The wrapper incorporates several advanced options from `astropy`, such as automatic or manual sampling in period/frequency, the ability to change the objective function for BLS, and the option to set the proposed eclipse durations for BLS.

These algorithms evaluate power at different frequencies to detect periodic signals in unevenly spaced data. By default, the LS algorithm uses a heuristic to choose these frequencies based on the observation baseline and the Nyquist frequency, although users can manually specify the frequencies if desired. At each frequency, a sinusoidal model is fitted, and power is computed based on the model's fit to the data. Conversely, the BLS algorithm fits a box-shaped model, representing a flat-bottomed dip, across a grid of periods, durations, and phases. The power is derived from the likelihood of the model. The power spectrum generated by these algorithms shows peaks at frequencies where the fit is strongest, indicating potential periodic signals.

The wrapper takes any number of light curves or radial velocities as input, if running on multiple light curves, each light curve is normalized by dividing by either the median or maximum flux value before sending it to the periodogram algorithm. Radial velocities across all requested data sets are combined and then normalized independently by the absolute maximum value for the primary and secondary stars, with the secondary then mirrored. After running the wrapper, the periodogram itself is returned and can be plotted, and the peak period is proposed for adoption.

7.1.2 RV Geometry

Analytical radial velocities (RVs) are fitted to Keplerian orbit, as discussed in Chapter 3, to estimate the eccentricity (e), argument of periastron (ω), systemic velocity (v_γ), and the time of superior conjunction ($t_{0,supconj}$), as well as the mass ratio (q), projected orbital semi-major axis (a_{orb}) for double-lined spectroscopic binaries (SB2s) or the single-component projected semi-major axis ($a_{comp,i}$) for single-lined spectroscopic binaries (SB1s).

Assuming the orbital period (P_{orb}) is known, we begin by binning the input data. A low-pass Savitzky-Golay filter (Savitzky u.a., 1964) is applied to smooth high-frequency noise. All estimates are based on per-component radial velocity equations as a function of true anomaly (ν).

$$\begin{aligned} RV_1(\nu) &= \frac{2\pi a_1 \sin i}{P_{\mathrm{orb}}\sqrt{1-e^2}}\left[e\cos\omega + \cos(\omega+\nu)\right] + v_\gamma \\ &= \frac{2\pi q a \sin i}{P_{\mathrm{orb}}(1+q)\sqrt{1-e^2}}\left[e\cos\omega + \cos(\omega+\nu)\right] + v_\gamma \end{aligned} \tag{7.1}$$

$$\begin{aligned} RV_2(\nu) &= -\frac{2\pi a_2 \sin i}{P_{\mathrm{orb}}\sqrt{1-e^2}}\left[e\cos\omega + \cos(\omega+\nu)\right] + v_\gamma \\ &= -\frac{2\pi a \sin i}{P_{\mathrm{orb}}(1+q)\sqrt{1-e^2}}\left[e\cos\omega + \cos(\omega+\nu)\right] + v_\gamma \end{aligned} \tag{7.2}$$

Initially, we estimate the mass ratio and systemic velocity in parallel, following the relationships observed in prior studies (Section 3.3).

$$v_\gamma = \frac{RV_1(\nu) + qRV_2(\nu)}{1+q} \tag{7.3}$$

$$q = \frac{RV_1(\nu) - v_\gamma}{-RV_2(\nu) + v_\gamma} \tag{7.4}$$

As we can see, v_γ and q appear in both expressions, which means we cannot uniquely determine them independently of each other. Thus, we iteratively compute them, starting with a rough estimate of q from the ratio of primary and secondary RV. If only one RV is available, q cannot be reliably estimated, so we estimate v_γ as the midpoint of the available RV. We can think of v_γ as the point in the RV curve where both components intersect.

With q and v_γ estimated, we compute the projected semi-major axis, a. We first estimate the semi-amplitudes from the available observations in each RV:

$$K_i = 0.5\left[\max(RV_i - v_\gamma) - \min(RV_i - v_\gamma)\right] \tag{7.5}$$

where index i = 1, 2 refers to the primary and secondary components, respectively. The corresponding projected semi-major axes are then:

$$a_i \sin i = \frac{K_i P_{\mathrm{orb}}}{2\pi\sqrt{1-e^2}} \tag{7.6}$$

Initially, we assume $e = 0$. If both RVs are available, $a = a_1 + a_2$.

Once q, v_γ and a are estimated, we fix them in the analytical radial velocities and fit for eccentricity and argument of periastron with a least-squares algorithm. We compute several solutions by iterating over a small grid of starting points with the combinations e_0 = [0, 0:4] and ω_0 = [0, $\pi/2$, π], ensuring the entire feasible parameter space is explored. Iterations continue until convergence within a specified tolerance or the maximum number of iterations is reached. After each iteration, the value of *asini* is recomputed with the updated eccentricity e and the solution is used as an initial point for the next iteration.

Finally, the phase of superior conjunction is estimated as the phase at which $v = v_\gamma$ and then converted to the time of superior conjunction, $t_{0,supconj}$.

7.1.3 LC Estimators

LC Geometry

The primary characteristic observed in light curves of eclipsing binary stars is the distinct dips in flux, resembling Gaussian bell curves during eclipses. This observation motivates the modeling of the light curve geometry. The procedure involves using Gaussian functions to model the eclipses and a cosine function to account for ellipsoidal variability due to tidal interactions. This approach can also approximate the light curve of a semi-detached binary system where one or both stars are partially or fully filling their Roche lobe. The two-Gaussian model implementation is based on (Mowlavi, N. u.a., 2017). The following description outlines the implementation of a two-Gaussian model.

The eclipses are modeled with Gaussian functions of the form

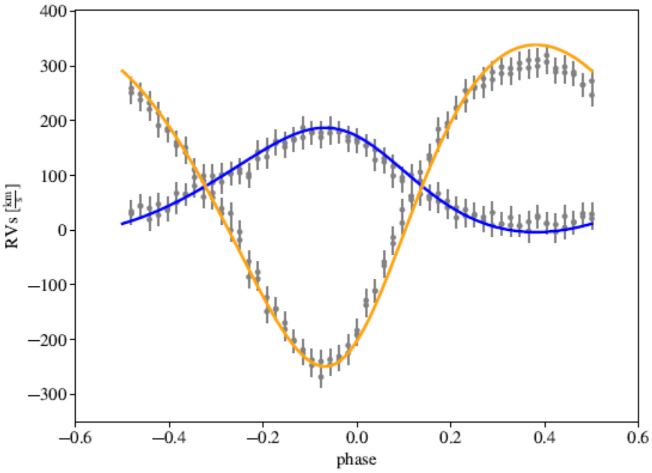

Figure 7.1: Analytic Keplerian radial velocity model fitted to a synthetic set of observations with the estimated orbital parameters obtained solely from the phase-folded radial velocity observations.

$$G_{\mu_i,d_i,\sigma_i}(\varphi) = d_i e^{-\frac{(\varphi-\varphi_i)^2}{2\epsilon_i^2}} \tag{7.7}$$

where index $i = 1, 2$ refers to the primary (deepest) and secondary (least deep) eclipses, respectively. The parameters μ_i, d_i, and σ_i correspond to the mean, depth, and standard deviation of the Gaussian functions, and φ represents the observation phase. The ellipsoidal-like variability is modelled as

$$\frac{1}{2}\, A_{ell}\; cos[4\pi(\varphi - \varphi_{0,ell}] \tag{7.8}$$

where A_{ell} is peak-to-peak amplitude of ellipsoidal-like variability, and φ_0, ell specifies whether cosine is centred on eclipse 1 ($\varphi_0, ell = \mu_1$) or eclipse 2 (($\varphi_0, ell = \mu_1$), The complete two-Gaussian model, including a constant C for baseline flux, is expressed as

$$G(\varphi) = C + \sum_{m=-2}^{2} G_{\varphi_1+m,d_1,\sigma_1}(\varphi) + \sum_{m=-2}^{2} G_{\varphi_2+m,d_2,\sigma_2}(\varphi) + \frac{1}{2} A_{\mathrm{ell}} \cos[4\pi(\varphi - \varphi_{0,\mathrm{ell}})] \tag{7.9}$$

This equation accounts for the periodic nature of the eclipses by including mirrored Gaussian components over a phase range from -2 to +2. Conventionally, the light curve is shifted so that the primary eclipse occurs at phase 0, setting $\mu_1 = 0$.

The two-Gaussian model is sensitive to the initial values of the model parameters. Thus, to ensure its convergence, `PHOEBE` first estimates the eclipse positions, widths, and depths using a simple algorithm that searches for the minimum of the light curve and isolates data in its vicinity that cross the median flux in phase (φ) space. All seven potential models (Table 7.1) are then fitted using a non-linear least-squares optimizer, and the best fit is chosen based on the highest Bayesian Information Criterion (BIC). The BIC is computed as (Feigelson u.a., 2012)

$$BIC = 2\ln L - p\ln N_{Obs} \tag{7.10}$$

where p is the number of model parameters (as detailed in Table 7.1) for each model, N_{Obs} is the number of observations, and $\ln L$ represents the log-likelihood.

Table 7.1: Two-Gaussian models used to describe eclipsing binary light curve geometries.

Model	Description	Number of Parameters
Two eclipses		
CG12	Without ellipsoidal-like var.	7
CG12E1	With ellipsoidal-like var. on eclipse 1	8
CG12E2	With ellipsoidal-like var. on eclipse 2	8
One eclipse		
CG	Without ellipsoidal-like var.	4
CGE	With ellipsoidal-like var. on eclipse 1	5
No eclipse		
CE	Ellipsoidal-like var.	3
C	Constant	1

The central positions of the Gaussians correspond to the eclipse positions ($\varphi_1 = \mu_1$). The eclipse durations w_i (expressed in phase) are defined as the widths of the Gaussian functions at a 2% magnitude depth relative to Gaussian depth d_i, given by

$$w_i = min(5.6\sigma_i, 0.4) \tag{7.11}$$

This upper limit of 0.4 prevents unphysically large eclipse durations for broad Gaussians. The Eclipse depths d_i are calculated as the difference between the brightest model magnitude and the magnitude at the bottom of the eclipse.

$$d_i = G_{max} - G(\varphi_i) \tag{7.12}$$

The constant C in Equation 7.9 equals G_{max} for detached eclipsing binaries without significant ellipsoidal variability.

The parameter ψ is computed iteratively using the Newton-Raphson method by solving $2\pi\Delta\Phi = \psi$ - $\sin\psi$, where $\Delta\Phi$ is the separation between the two eclipses in phase space. The eccentricity e argument of periastron ω, and time of superior conjunction $t_{0,supconj}$ are then estimated as follows:

eccentricity:

$$e = [\sin^2(\frac{\psi - \varphi}{2}) + (\frac{w_2 - w_1}{w_2 + w_1})^2 \cos^2(\frac{\psi - \varphi}{2})]^{1/2} \tag{7.13}$$

argument of periastron:

$$\omega_1 = \arcsin(\frac{1}{e}\frac{w_2 - w_1}{w_2 + w_1}) \tag{7.14}$$

$$\omega_2 = \arccos(\frac{\sqrt{1-e^2}}{e\tan(\frac{\psi-\varphi}{2})}) \tag{7.15}$$

$$\omega = \begin{cases} \omega_2, & \text{if } \omega_1 \geq 0 \\ 2\pi - \omega_2, & \text{if } \omega_1 < 0 \end{cases} \tag{7.16}$$

time of superior conjunction:

$$t_{0,supconj} = t_{0,supconj,orig} + \varphi_1 P_{Orb} \tag{7.17}$$

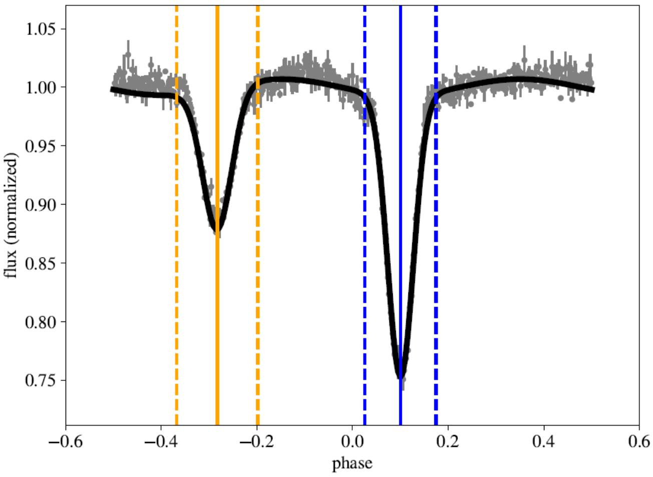

Figure 7.2: Two-Gaussian model used to determine the phases of eclipse minima, ingress, and egress (blue and orange vertical lines representing the primary and secondary eclipses, respectively), as well as the input binned synthetic observations.

EBAI

The 2.4 release of `PHOEBE` supports two methods - 'mlp', which uses a trained neural network (Prša u.a., 2008), and 'knn', which uses a trained K-nearest neighbors regressor model.

The input light curves are normalized and fitted with a two-Gaussian model to estimate eclipse positions and widths. This analytical representation is then sampled at 201 phase points as the training set and is passed to the feed-forward network with pre-trained weights using 201 input units, 40 hidden units, and 5 output units to propose values for parameters: $T_{eff,2}/T_{eff,1}$, $(R_{equiv,1}{+}R_{equiv,2}/a_{orb})$, $e\sin\omega_0$, $e\cos\omega_0$, and i, in addition to $t_{0,supconj}$ computed from phase-shift applied using two-Gaussian model.

7.2 Merit Function

To solve the inverse problems, we need synthetic forward model outcomes to compare them with the observed data. This requires a quantitative way, merit function, to make a comparison. Below we define the components of the merit function related to `PHOEBE` (Conroy u.a., 2020).

lnpriors: It is defined as the logarithm of the probability of drawing the current face values, p, from the prior distributions π which are either known (or physically motivated) for the system (see (Kass u.a., 1996)), i.e.,

$$\text{lnpriors} = \sum_{\text{priors}} \ln(\mathrm{P}(p|\Pi)) \tag{7.18}$$

residuals: It is defined as the difference between the value observed and the value for the synthetic model for each observation time (or masked time) of the observable

$$\text{residuals} = y_0(t_{\text{masked}}) - y_m(t_{\text{masked}}) \tag{7.19}$$

where y_0 is the observed value and y_m is the value used to get the synthetic model.

chi2 (χ^2): In `PHOEBE`, χ^2 is defined as the sum of squares of residuals of all the data points for the given observable computed across all the datasets over the squares of the provided per point uncertainties plus σ_0 which is added to handle uncertainty underestimation from the provided observed uncertainties. If the provided uncertainties are believed to be underestimated, then the uncertainty underestimation term, σ_{lnf}, can be optimized or sampled. In the default setting, $\sigma_{\text{lnf}} = -\infty$.

$$\chi^2 = \sum_{\text{datasets}} \frac{(y_0 - y_m)^2}{\sigma^2} + \ln(\sigma^2) \tag{7.20}$$

where

$$\sigma^2 = \sigma_0^2 + y_m^2 e^{2\sigma_{\text{lnf}}}. \tag{7.21}$$

lnlikelihood: It is defined as half the value of the negative of the χ^2 value, i.e.,

$$\text{lnlikelihood} = -0.5\chi^2 \tag{7.22}$$

lnprobability:

It is defined as the sum of lnpriors and lnlikelihood, In the absense of priors, this becomes analogous to χ^2. In `PHOEBE`, -lnprobability is used as the default merit function. The optimal model is found by maximizing the log-probability.

$$\text{lnprobability} = \text{lnpriors} + \text{lnlikelihood}. \tag{7.23}$$

7.3 Optimizers

`PHOEBE` includes wrappers around several from `scipy.optimize` (Virtanen u.a., 2020), such as Nelder-Mead downhill simplex (Gao u.a., 2012), differential evolution, Powell, and the conjugate gradient. These optimizers are quite efficient in refining model fit once already in the vicinity of the solution found via estimators.

`PHOEBE` provides flexibility in choosing the parameters to be adjusted by the optimizer and offers the option to define priors if desired. It is important to note that, irrespective of whether the user provides priors or not, the inherent parameter limits, and wrapping limits act as uninformative priors, effectively penalizing the merit function outside these bounds, ensuring that the optimization stays within the meaningful regions of the parameter space.

Among the available methods, the Nelder Mead method is often the most efficient when derivatives are unreliable, as it relies solely on function evaluations and cannot diverge locally. This robustness contrasts with the differential corrections (DC) method employed in the Wilson-Devinney (WD) code for binary star modeling. While WD's DC algorithm is known for its speed and efficiency when the discrepancy between the observed and computed curves is relatively small, it can sometimes diverge locally, failing to distinguish between local and global minima, a common issue with pure gradient-based methods that rely heavily on local derivative information.

The Nelder Mead method iteratively generates a sequence of simplices to approximate an optimal point. A simplex, in n dimensions, is a polytope with $n + 1$ vertices, each representing a point in n-dimensional parameter space. At each iteration, the vertices of the simplex are ordered by their objective function values, with the vertex having the lowest function value considered the best. During each iteration, the algorithm attempts to improve the solution by modifying the vertex with the highest function value through geometric transformations: reflection, expansion, contraction, or shrink. These operations allow the simplex to move through the parameter space towards a local minimum, refining the solution iteratively until the simplex contracts around an optimal point.

By not relying on gradients, Nelder-Mead is less prone to being stuck in local minima. However, it also faces challenges in ensuring global optimality, especially in parameter spaces that are flat around the global minimum with lots of local minima. The choice of initial simplex and the scale of the parameter space can significantly influence the convergence and the quality of the solution found.

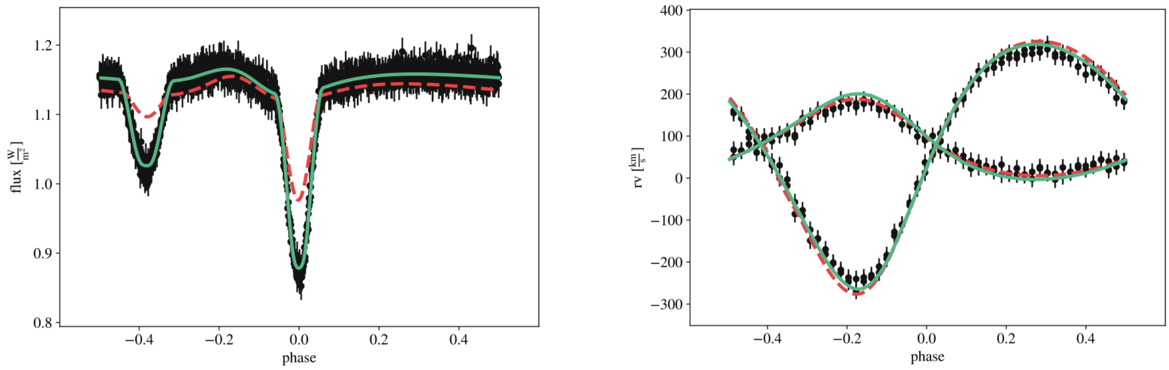

Figure 7.3: Model improvement after adopting proposals from estimators (dashed red lines) and after running Nelder-Mead (solid green lines).

7.4 Samplers

Samplers are not designed to find the global solution, rather, to explore the parameter space and provide robust posteriors and uncertainties that expose the underlying correlations and degeneracies between various parameters.

7.4.1 Markov Chain Monte Carlo (emcee)

Markov Chain Monte Carlo (MCMC) methods are a class of algorithms used to sample from the posterior probability density $p(\Theta|D)$. In Bayesian inference, the posterior distribution combines our prior beliefs $p(\Theta)$ about the parameters Θ with the likelihood $p(D|\Theta)$ of observing the data D, according to Bayes' theorem,

$$p(\Theta|D) = \frac{1}{Z}p(\Theta)p(D|\Theta) \tag{7.24}$$

where the normalization $Z = p(D)$, known as the evidence, is given by

$$Z = \int p(D|\Theta)p(\Theta)d\Theta \tag{7.25}$$

Computing evidence Z directly involves integrating over all possible parameter values, which is often computationally intractable, especially in high-dimensional spaces. However, it is possible to sample from $p(\Theta|D)$ without explicitly computing Z using MCMC methods. These methods generate a sequence of random samples, known as a Markov chain, whose stationary distribution is the target distribution we wish to sample from, typically the posterior distribution in Bayesian inference.

Each point in a Markov chain $X(t_i) = [\Theta_i]$ depends only on the position of the previous state $X(t_{i-1})$, a property known as the Markov property. As the Markov chain progresses, the samples gradually represent the posterior distribution. Thus, MCMC methods effectively approximate the posterior distribution without the need to directly calculate the evidence Z. These samples can be used to evaluate an integral over the variable, such as its expected value or variance.

The Metropolis-Hastings (M-H) algorithm is a widely used implementation of MCMC methods. This algorithm involves proposing a new sample position Y given the current position $X(t)$ from a transition distribution $Q(Y; X(t))$. The proposed sample Y is either accepted or rejected with the acceptance probability

$$\min(1, \frac{p(Y|D)}{p(X(t)|D)} \frac{Q(X(t); Y)}{Q(Y; X(t)} \tag{7.26}$$

The transition distribution $Q(Y; X(t))$, also known as the proposal distribution, is the probability distribution for the proposal Y given the current position X(t). A common choice for $Q(Y; X(t))$ is a multivariate Gaussian distribution centered on $X(t)$ with a covariance matrix that can be tuned for performance.

The acceptance ratio $p(Y|D)/p(X(t)|D)$ compares the likelihood of the proposed and current states under the target distribution. Meanwhile, the ratio $Q(X(t); Y)/Q(Y; X(t))$ adjusts for any asymmetry in the proposal distribution. If proposal Y is accepted, then the new position is set to Y (i.e., $X(t + 1) = Y$) Otherwise, the chain remains at the current position $X(t + 1) = X(t)$. The acceptance decision is stochastic, a random value

u is drawn from a uniform distribution $U(0, 1)$, and the proposal is accepted if the value u is less than or equal to the acceptance probability.

The samples obtained through this method are typically autocorrelated, as each sample depends on the previous one. This autocorrelation can be reduced by techniques such as burn-in(discarding initial samples to allow the chain to stabilize), thinning(keeping every k-th sample) or adjusting the proposal distribution to achieve an appropriate acceptance fraction, generally between 0.2 and 0.5, by tuning its covariance matrix.

Goodman & Weare (Goodman u.a., 2010) proposed an affine-invariant ensemble sampling algorithm that significantly outperforms the standard M-H algorithm by producing independent samples with a much shorter autocorrelation time. This method involves simultaneously evolving an ensemble of K walkers $S = X_k$ where the proposal distributions for one walker k is based on the current positions of the $K - 1$ walkers in the complementary ensemble $S_{[k]} = X_j, \forall j \neq k$. Each walker is represented as a vector in the N-dimensional real-valued parameter space.

To update the position of a walker at position X_k, a walker X_j is drawn randomly from the remaining walkers $S_{[k]}$ and a new position Y then is proposed as

$$X_k(t) \rightarrow Y = X_j + Z[X_k(t) - X_j] \tag{7.27}$$

where Z is a random variable drawn from a distribution $g(Z = z)$. Goodman & Weare advocate a specific form of $g(z)$, given by

$$g(z) \propto \begin{cases} \frac{1}{\sqrt{z}} & \text{if} z \in [\frac{1}{a}, a], \\ 0 & \text{otherwise} \end{cases} \tag{7.28}$$

where a is an adjustable scale parameter, typically set to 2. The proposal is either accepted or rejected with probability

$$q = \min(1, Z^{N-1} \frac{p(Y|D}{p(X(t)|D} \tag{7.29}$$

where N is the dimension of the parameter space, this procedure is repeated for each walker in the ensemble in sequence.

`PHOEBE` includes a wrapper around EMCEE (Foreman-Mackey u.a., 2013), a Python package that implements the Affine-Invariant Ensemble Sampling algorithm. When preparing an EMCEE run through `PHOEBE`, users can define the distributions for the priors. it is generally good practice to start EMCEE in an N-dimensional hyperball (e.g., using Gaussian distributions on multiple parameters) centered around the best-known solution from optimization (Section 7.3).

In addition to setting distributions, users can set options for the number of processors, walkers, and iterations. After the run is complete, or at intermediate steps as requested, users can view the progress of the chains and the log probability versus iteration. This allows adjustment of the burn-in and thinning parameters as necessary. If the run is completed but convergence has not been achieved, `PHOEBE` allows for the continuation of an emcee run from the existing chains.

`PHOEBE` automatically determines defaults for thinning and burn-in based on the autocorrelation times of the chains

$$burnin = F_{burnin} \max(\tau_{autocorr}) \tag{7.30}$$
$$thin = F_{thin} \min(\tau_{autocorr}) \tag{7.31}$$

where F_{burnin} and F_{thin} are user-defined scaling factors that default to 2 and 0.5, respectively, and $\tau_{autocorr}$ represent the estimated autocorrelation times, per-parameter, as exposed by EMCEE.

7.5 Posteriors & Uncertainties

Once the chains sufficiently cover the parameter space and are considered to be converged, users can adjust the thinning, and burn-in to apply to the chains returned by EMCEE and generate a multivariate distribution of the resulting posteriors. Posterior distribution not only represents the uncertainties on each of the sampled parameter values but also the correlations between all of the sampled parameters. When these distributions are sufficiently Gaussian, the posteriors can easily be converted into a multivariate Gaussian distribution which represents the posteriors as just the means and a covariance matrix. These posteriors can be propagated through the constraints and exposed in any desired parameterization.

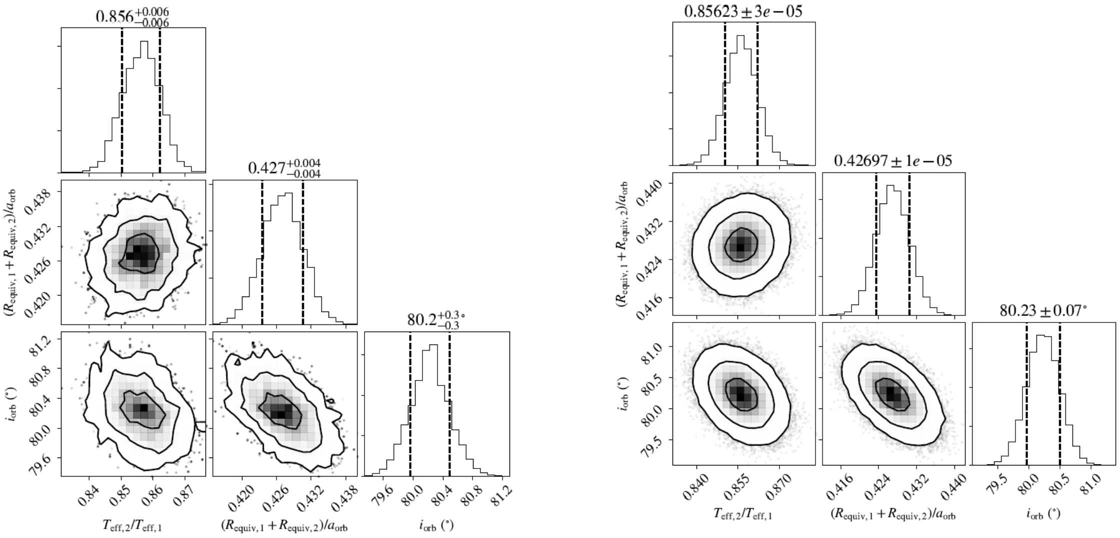

Figure 7.4: An example corner plot of the (burn-in and thinning applied) posteriors directly from emcee results (left). These can optionally be translated into a multivariate Gaussian distribution (right), which represents the same information with only the means and covariance matrix when appropriate.

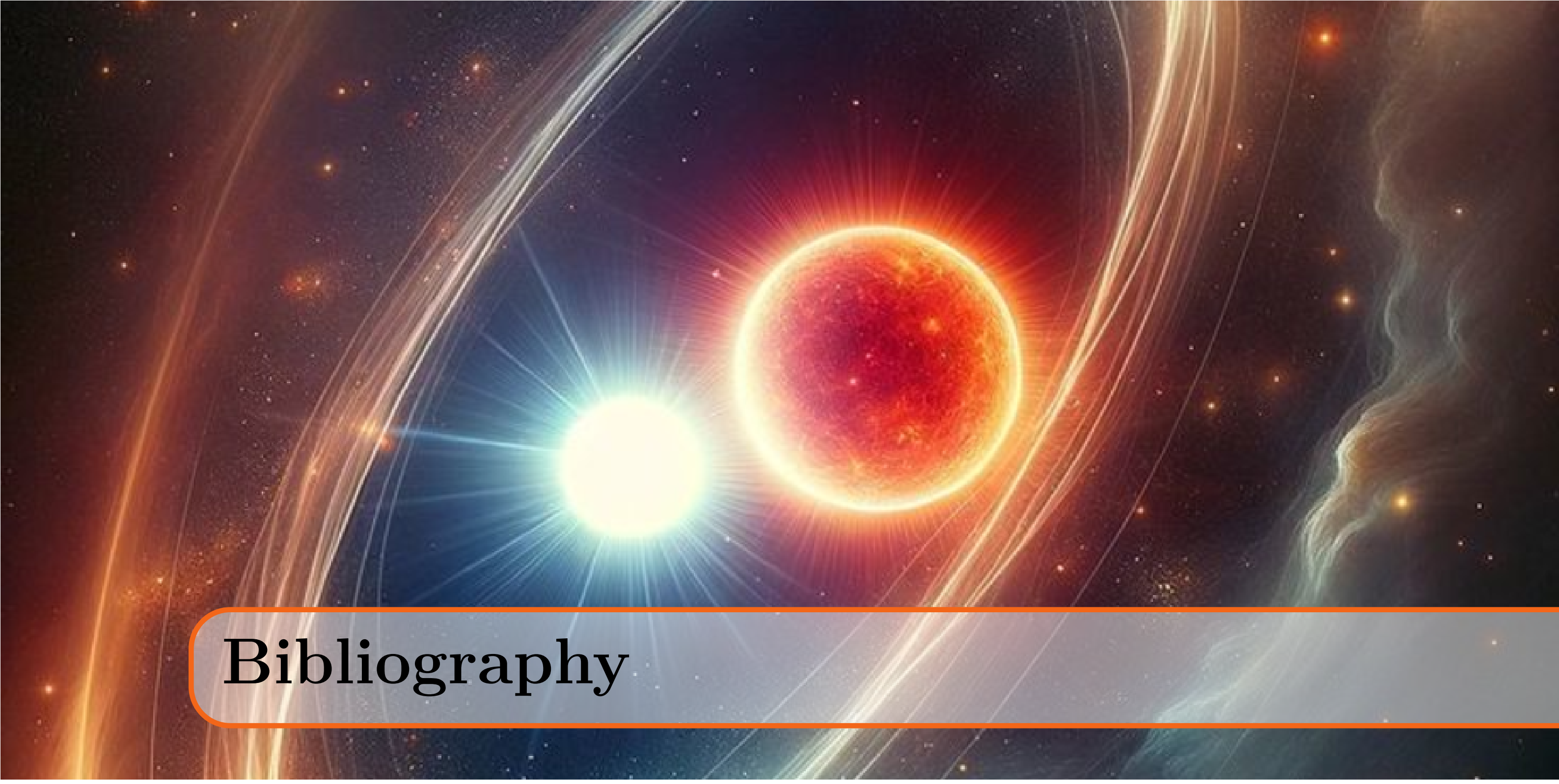

Bibliography

Michell, John(1767): *An Inquiry into the Probable Parallax, and Magnitude of the Fixed Stars, from the Quantity of Light Which They Afford us, and the Particular Circumstances of Their Situation, by the Rev. John Michell, B. D. F. R. S.*234–264.

Herschel, William(1802): *Catalogue of 500 New Nebulae, Nebulous Stars, Planetary Nebulae, and Clusters of Stars; With Remarks on the Construction of the Heavens*477–528.

Savitzky, Abraham. / Golay, M. J. E.(1964): *Smoothing and Differentiation of Data by Simplified Least Squares Procedures.*, 8: 1627-1639.

Trimble, Virginia L. / Thorne, Kip S.(1969): *Spectroscopic Binaries and Collapsed Stars*1013.

Bell, S. A. / Hilditch, R. W. / Adamson, A. J.(1987): *A photometric and spectroscopic study of the early-type binary V1182Aquilae.*961-983.

Heintz, W. D.(1988): *THE CASTOR SYSTEM*, 629: 834.

Batten, Alan H.(1989): *Two Centuries of Study of Algol Systems*, 1-2: 1-8.

Bonnell, Ian A.(1994): *A new binary formation mechanism*, 3: 837-848.

Kass, Robert E. / Wasserman, Larry A.(1996): *The Selection of Prior Distributions by Formal Rules*1343-1370.

Bate, Matthew R. / Bonnell, Ian A. / Bromm, Volker(2003): *The formation of a star cluster: predicting the properties of stars and brown dwarfs*, 3: 577-599.

Siebert, Harald(2005): *The early search for stellar parallax: Galileo, Castelli, and Ramponi*251-271.

Prša, A. / Guinan, E. F. / Devinney, E. J. / DeGeorge, M. / Bradstreet, D. H. / Giammarco, J. M. / Alcock, C. R. / Engle, S. G.(2008): *Artificial Intelligence Approach to the Determination of Physical Properties of Eclipsing Binaries. I. The EBAI Project*, 1: 542.

Albrecht, Simon / Reffert, Sabine / Snellen, Ignas AG / Winn, Joshua N(2009): *Misaligned spin and orbital axes cause the anomalous precession of DI Herculis*, 7262: 373–376.

Claret, A / Torres, G / Wolf, M(2010): *DI Herculis as a test of internal stellar structure and general relativity-New apsidal motion rate and evolutionary models*A4.

Mamajek, Eric E. / Kenworthy, Matthew A. / Hinz, Philip M. / Meyer, Michael R.(2010): *Discovery of a Faint Companion to Alcor Using MMT/AO 5 μm Imaging*, 3: 919-925.

Goodman, Jonathan / Weare, Jonathan(2010): *Ensemble samplers with affine invariance*, 1: 65-80.

Offner, Stella S. R. / Kratter, Kaitlin M. / Matzner, Christopher D. / Krumholz, Mark R. / Klein, Richard I.(2010): *THE FORMATION OF LOW-MASS BINARY STAR SYSTEMS VIA TURBULENT FRAGMENTATION*, 2: 1485–1494.

Kraus, Adam L. / Ireland, Michael J.(2011): *LkCa 15: A YOUNG EXOPLANET CAUGHT AT FORMATION?*, 1: 5.

Matijevič, G. u.a.(2011): *Single-lined Spectroscopic Binary Star Candidates in the RAVE Survey*, 6: 200.

Southworth, John(2012): *Eclipsing Binary Stars: the Royal Road to Stellar Astrophysics*.

Gao, Fuchang / Han, Lixing(2012): *Implementing the Nelder-Mead simplex algorithm with adaptive parameters*, 1: 259-277.

The Astropy Collaboration u.a.(2013): *Astropy: A community Python package for astronomy*A33.

Foreman Mackey, Daniel / Hogg, David W. / Lang, Dustin / Goodman, Jonathan(2013): *emcee: The MCMC Hammer*, 925: 306.

Duchêne, Gaspard / Kraus, Adam(2013): *Stellar Multiplicity*, 1: 269-310.

Tkachenko, A.(2015): *Probing high-mass stellar evolutionary models with binary stars*In: New Windows on Massive Stars200-205.

Mowlavi, N. u.a.(2017): *Gaia eclipsing binary and multiple systems - Two-Gaussian models applied to OGLE-III eclipsing binary light curves in the Large Magellanic Cloud* A92.

Trimble, Virginia / Thorne, Kip S.(2018): *Spectroscopic Binaries and Collapsed Stars: Part II*arXiv:1811.04310.

Southworth, John(2020): *Binary stars: a cheat sheet*.

Conroy, Kyle E. u.a.(2020): *Physics of Eclipsing Binaries. V. General Framework for Solving the Inverse Problem*, 2: 34.

Virtanen, Pauli u.a.(2020): *SciPy 1.0: fundamental algorithms for scientific computing in Python*, 3: 261-272.

Heyne, T. u.a.(2020): *Spectroscopic characterization of nine binary star systems as well as HIP 107136 and HIP 107533*, 1: 99-117.

Meunier, Nadège(2021): *Stellar variability in radial velocity*arXiv:2104.06072.

Peled, Gil / Volansky, Tomer(2022): *Constraining Dark Matter Inside Stars Using Spectroscopic Binaries and a Modified Mass-Luminosity Relation*arXiv:2203.09522.

Merle, Thibault(2024): *Dancing with the Stars: a Review on Stellar Multiplicity*, 2: 170-214.

Kaushik, Mahima / Mattoo, Aditee / Rastogi, Ritesh(2024): *Exoplanet Detection : A Detailed Analysis*arXiv:2404.09143.

Anchordoqui, Luis *Celestial Mechanics*
`https://www.lehman.edu/faculty/anchordoqui/chapter25.pdf`.

Benacquista, Matthew (2013): *An Introduction to the Evolution of Single and Binary Stars.* , Springer New York.

Burnham, Robert (1978): *Burnham's celestial handbook. an observers guide to the universe beyond the solar system.* .

contributors, Wikipedia (2023): *Binary star*
, [Online; accessed 21-June-2024].

El Badry, Kareem (2024): *Gaia's binary star renaissance*
.

Endl, Michael / Cochran, William D. (2007): *CHAPTER 47 - Extrasolar Planets.* In: McFadden, Lucy Ann / Weissman, Paul R. / Johnson, Torrence V. (Hg.), Encyclopedia of the Solar System (Second Edition). San DiegoAcademic Press: 887-902.

Feigelson, Eric D. / Babu, G. Jogesh (2012): *Modern Statistical Methods for Astronomy: With R Applications.* , Cambridge University Press.

Kratter, Kaitlin M. (2011): *The Formation of Binaries*
.

Lovis, C. / Fischer, D. (2010): *Radial Velocity Techniques for Exoplanets.* In: Seager, S. (Hg.), Exoplanets.: 27-53.

Index

A

Astrophysical Significance 43

B

Binary Star Systems 9–12

E

Estimation of parameters 45

I

Introduction 39

O

Observations 44

S

Some important Space Missions About Eclipsing Binares 40

T

Types of Eclipsing Binaries 40